Megaron, Vol. 21, No. 3, pp. 296–320, September 2026

Megaron
https://megaron.yildiz.edu.tr - https://megaronjournal.com
DOI: https://doi.org/10.14744/megaron.2026.24922

Article

Mapping heat vulnerability in Esenler, Istanbul using equal and entropy weighting: A multi-dimensional GIS approach

Elnaz Tajer, Kaan Ozgun

Ozyegin University, Faculty of Architecture And Design, Istanbul, Türkiye

ARTICLE INFO

Article history
Received: 27 October 2025
Revised: 1 July 2026
Accepted: 11 July 2026

Key words:
Heat Vulnerability Index (HVI); urban heat exposure; entropy weighting method; esenler district; spatial analysis; climate adaptation.

ABSTRACT

Urban heat vulnerability is an emerging challenge for rapidly densifying cities, where socio-economic inequalities intersect with physical exposure. This study assesses neighborhood-level heat vulnerability in Esenler District, Istanbul, by integrating environmental and socio-demographic indicators within a composite Heat Vulnerability Index (HVI). Using satellite-derived indicators, including Land Surface Temperature (LST), Normalized Difference Vegetation Index (NDVI), and Normalized Difference Built-up Index (NDBI), combined with socio-economic and adaptive capacity measures, the analysis applies both Equal Weighting and Entropy Weighting Methods to evaluate spatial variability and methodological robustness. Results reveal significant intra-district disparities, with HVI values ranging from 0.15 to 0.69 ($\Delta = 0.54$). The majority of neighborhoods (15 of 17) fall within the high-vulnerability category, representing approximately 96% of the population, while only one neighborhood exhibits low vulnerability and one shows moderate vulnerability. The strong correlation ($r = 0.94$) between Equal and Entropy-weighted results confirms the index's methodological stability. Spatial clustering of high vulnerability in central Esenler underscores how dense urban morphology and social disadvantage co-produce climatic risk. This study addresses a critical gap in Istanbul's urban climate literature by providing one of the first data-driven, neighborhood-scale HVI applications. A Heat Vulnerability–Adaptive Capacity matrix translates results into a neighborhood-level prioritization scheme, identifying critical hotspots (N3, N7, N10) for immediate adaptation. Integrating entropy-based weighting enhances the interpretation of diverse environmental and social datasets, offering a replicable model for other contexts. The results emphasize targeted adaptation measures such as expanding green infrastructure, improving thermal comfort, and prioritizing vulnerable communities.

Cite this article as: Tajer, E., & Ozgun, K. (2026). Mapping heat vulnerability in Esenler, Istanbul using equal and entropy weighting: A multi-dimensional GIS approach. Megaron, 21(3):296–320.

***Corresponding author**
*E-mail address: elnaz.tajer@ozu.edu.tr

Published by Yıldız Technical University, İstanbul, Türkiye
This is an open access article under the CC BY-NC license (http://creativecommons.org/licenses/by-nc/4.0/).

INTRODUCTION

Rapid urbanization has intensified the frequency and severity of extreme heat events, posing significant threats to human health, ecosystems, and urban infrastructure (Chen et al., 2025b; Wang et al., 2024). The Intergovernmental Panel on Climate Change (IPCC, 2022) projects that global mean surface temperature will likely exceed the 1.5 °C threshold within the next two decades, amplifying the frequency, duration, and severity of heatwaves (Chen et al., 2025a). The Urban Heat Island (UHI) effect exacerbates these risks, as built-up areas absorb and retain more heat than surrounding rural regions (Shen et al., 2025; Leal Filho et al., 2018). Conversion of vegetated, permeable surfaces into impervious construction materials alters the surface energy balance, driving persistent microclimatic changes (Patel et al., 2024). Consequently, urban residents face prolonged heat stress, which elevates health risks (Hossain et al., 2024), reduces labor productivity (Kimmich et al., 2025; Lai et al., 2023), and exacerbates social inequalities (Macharia & Kiage, 2025; Leal Filho et al., 2018). Growing evidence indicates that heat-related impacts are distributed unequally, with low-income populations, older adults, and children disproportionately affected (Uejio et al., 2024). Heat vulnerability thus emerges from the intersection of environmental exposure, socio-demographic sensitivity, and adaptive capacity, where limited access to green infrastructure and public services magnifies local thermal stress (Lopes et al., 2025; Li et al., 2024). Addressing these interconnected challenges requires integrating spatial risk mapping with socio-economic support systems, ensuring that adaptation measures are both data-driven and socially equitable (Randazza et al., 2023; Berisha et al., 2017). Because these interactions occur unevenly across space, neighborhood-scale assessments are crucial for identifying localized risk patterns and supporting targeted adaptation (Ho et al., 2025; Cangüzel & Coşkun Hepcan, 2024).

These patterns are particularly pronounced in Istanbul, one of Europe's fastest-growing megacities. Uncontrolled urban sprawl, high building density, and loss of natural land cover have produced temperature contrasts exceeding 4 °C between urban and rural zones (Kuru & Okay, 2025; Sari et al., 2025; Okumuş & Terzi, 2021). Within the city, Esenler exemplifies the convergence of intense UHI effects and socio-economic vulnerability. Home to over 427,000 residents distributed across 17 neighborhoods (TÜİK, 2023), it combines extreme density, minimal vegetation, and limited public space. Remote-sensing studies consistently identify Esenler as one of Istanbul's warmest districts (Khorrami & Gündüz, 2019; Zaeemdar & Baycan, 2017). Dogru et al. (2019) described its compact, poorly ventilated morphology and low environmental quality, linked to informal housing, limited education, and restricted healthcare access. Children under fifteen account for more than 20 % of the population, amplifying health risks from heat and pollution. Consequently, Esenler ranks 36th out of 39 districts in Istanbul's Quality-of-Life Index (Şeker et al., 2022). These conditions make Esenler a representative case for investigating neighborhood-scale heat vulnerability in the context of a Mediterranean megacity. Moreover, its social composition provides an opportunity to explore how spatially explicit vulnerability mapping can inform equitable Heat Action Planning and community-based adaptation.

Recent empirical research has revealed Istanbul's escalating thermal stress. Sari et al. (2025) recorded Physiologically Equivalent Temperature (PET) values exceeding 45 °C during the 2021 heatwave, while Yılmaz et al. (2024) confirmed that compact districts experience substantially higher heat stress than vegetated zones. Anticipated increases in heat-related mortality, particularly among elderly residents and women, highlight the city's need for targeted adaptation (Yılmaz et al., 2024). Furthermore, uneven access to green infrastructure perpetuates a "green divide" between redeveloped and older neighborhoods (Yazar et al., 2023). Such disparities illustrate how rapid urbanization and socio-economic inequality jointly exacerbate environmental risks (Yılmaz et al., 2024). These interlinked vulnerabilities position Esenler as a critical testbed for evaluating integrated approaches to urban heat resilience. By linking environmental exposure with social sensitivity and adaptive capacity, this study contributes to an emerging body of research advocating equitable, data-informed climate adaptation.

Heat Vulnerability Index (HVI)

HVI, grounded in the IPCC's framework of exposure, sensitivity, and adaptive capacity (IPCC, 2014; IPCC, 2022), offers a multidimensional means of identifying populations most at risk from extreme heat (Chen et al., 2025b). Environmental exposure is typically quantified through indicators such as land surface temperature (LST), vegetation (NDVI), and built-up density (NDBI). Sensitivity captures demographic and socio-economic factors such as age distribution, gender, and education (Chen et al., 2025a; Li et al., 2025; Parker et al., 2025; Zeng et al., 2022), while adaptive capacity reflects access to green space, healthcare, and social infrastructure (Munoz-Pizza et al., 2023; Li et al., 2025). Together, these dimensions generate spatially explicit vulnerability maps that inform climate-adaptation policies and public health planning.

Despite their value, HVI frameworks remain methodologically heterogeneous, differing in indicator selection, weighting, and spatial granularity (Parker et al., 2025; Chen et al., 2025b). Among weighting techniques, Equal Weighting and Principal Component Analysis (PCA) dominate due to simplicity and reproducibility (Cheng et al., 2021; Li et al., 2022). Expert-based methods such as the Analytic Hierarchy Process (AHP) incorporate subjective judgment, while data-driven alternatives like the Entropy

Weighting Method (EWM) derive indicator weights from statistical information content, reducing human bias (Yang & Zhao, 2023). EWM is particularly effective for neighborhood-scale analyses that integrate diverse environmental and socio-economic datasets (Guo et al., 2024). Although the selection and categorization of indicators vary across contexts, spatial scales, and data availability, neighborhood-scale HVI applications consistently integrate multiple dimensions to capture local heterogeneity in exposure, sensitivity, and adaptive capacity (Li et al., 2025; Parker et al., 2025; Chen et al., 2025b).

Research Gap and Objectives

Previous studies in Istanbul can be broadly grouped into two categories. First, several studies have examined urban heat island dynamics and the influence of land-use change, urban morphology, and vegetation patterns on urban temperatures (Kuru & Okay, 2025; Sari et al., 2025; Yılmaz et al., 2024). Second, more recent research has applied integrated heat vulnerability assessment frameworks that combine environmental and socio-demographic indicators at the metropolitan scale (Okumuş, 2025). While these studies have advanced understanding of urban heat risks in Istanbul, neighbourhood-level analyses within specific high-risk districts remain scarce, limiting the spatial resolution available for targeted adaptation planning. In particular, studies that simultaneously integrate exposure, sensitivity, and adaptive capacity at the neighbourhood scale are still lacking. Esenler, with its high density, limited greenery, and socio-economic disparities, provides an ideal context for applying such a framework at the intra-district level. Moreover, although various global studies have compared weighting schemes, including Equal Weighting, Entropy Weighting, PCA, and AHP, no empirical comparison of these methods has been conducted in Istanbul's urban context. Building on these gaps, this study represents the first neighborhood-scale HVI for Istanbul that assesses the robustness of results using both subjective (Equal Weighting) and objective (Entropy Weighting) approaches. By integrating environmental exposure, socio-demographic sensitivity, and adaptive capacity into a unified IPCC-based framework, it provides both contextual and methodological advancements in assessing urban heat vulnerability. Specifically, the study addresses the following research questions:

Q1: Which neighborhoods in Esenler are most vulnerable to UHI effects when environmental exposure, socio-demographic sensitivity, and adaptive capacity are considered together?

Q2: How do different weighting approaches (Equal Weighting vs. Entropy Weighting Method) influence the assessment of heat vulnerability at the neighborhood scale?

Q3: Which neighborhoods should be prioritized for climate adaptation interventions based on the combined assessment of heat vulnerability and adaptive capacity?

MATERIALS AND METHODS

Study area

Esenler (41.06°N, 28.86°E), located approximately 18 km west of the Bosporus on Istanbul's European side, covers an area of 18.43 km² and had a population of 454,569 in 2023 (Turkish Statistical Institute [TÜİK], 2023) (Figure 1). The district exhibits a compact urban form, high residential density, and limited publicly accessible green spaces, all of which contribute to elevated surface temperatures and a pronounced UHI effect (Okumuş & Terzi, 2021; Dogru et al., 2019; Zaeemdar & Baycan, 2017). As one of Istanbul's most densely populated districts, Esenler is characterized by intense residential concentration and urban congestion, conditions that can exacerbate urban heat accumulation and exposure (Sari et al., 2022). Socio-economic characteristics, including low household incomes and moderate educational attainment, further reduce residents' adaptive capacity to heat stress (Dogru et al., 2019). In terms of socio-economic structure, 75% of the population belongs to the low-income group, while the remaining 25% falls within the middle-income category (Sari et al., 2022). These conditions illustrate heightened sensitivity to environmental stressors and restricted adaptive capacity at the household level.

Esenler is administratively divided into 17 neighborhoods, the smallest administrative units considered in this study. Neighborhood-level socio-demographic data, including population, population density, age distribution (% children under five and % elderly ≥65), female population percentage, literacy rates, educational attainment (basic and higher education), and per-capita household income, were compiled to capture intra-district variability (Table 1). Unusually low population densities in neighborhoods such as Çifte Havuzlar (18.7 persons/ha) and Oruçreis (39.45 persons/ha) reflect specific land use characteristics, including university campuses and military zones, respectively. In contrast, densely populated neighborhoods such as Fatih reach 810.8 persons/ha, reflecting the district's heterogeneous urban structure. Per-capita household income ranges from TL 13,290 in Tuna to TL 18,717 in Davutpaşa. Household income data were obtained from Endeksa in 2025 and are reported as estimated monthly per-capita income (TL/person/month) at the neighborhood level. During the data collection period, the net monthly minimum wage in Türkiye was 22,104 TL (Ministry of Labour and Social Security, 2024). Estimated neighborhood income values ranged from 13,290 to 18,710 TL/person/month. Although per-capita income and minimum wage are not directly comparable measures, the observed values provide contextual evidence of relatively limited economic resources across the study area, which may constrain households' capacity to cope with heat-related risks. At the same time, the proportions of children under five and elderly residents also vary across neighborhoods, highlighting demographic differences relevant to heat vulnerability.

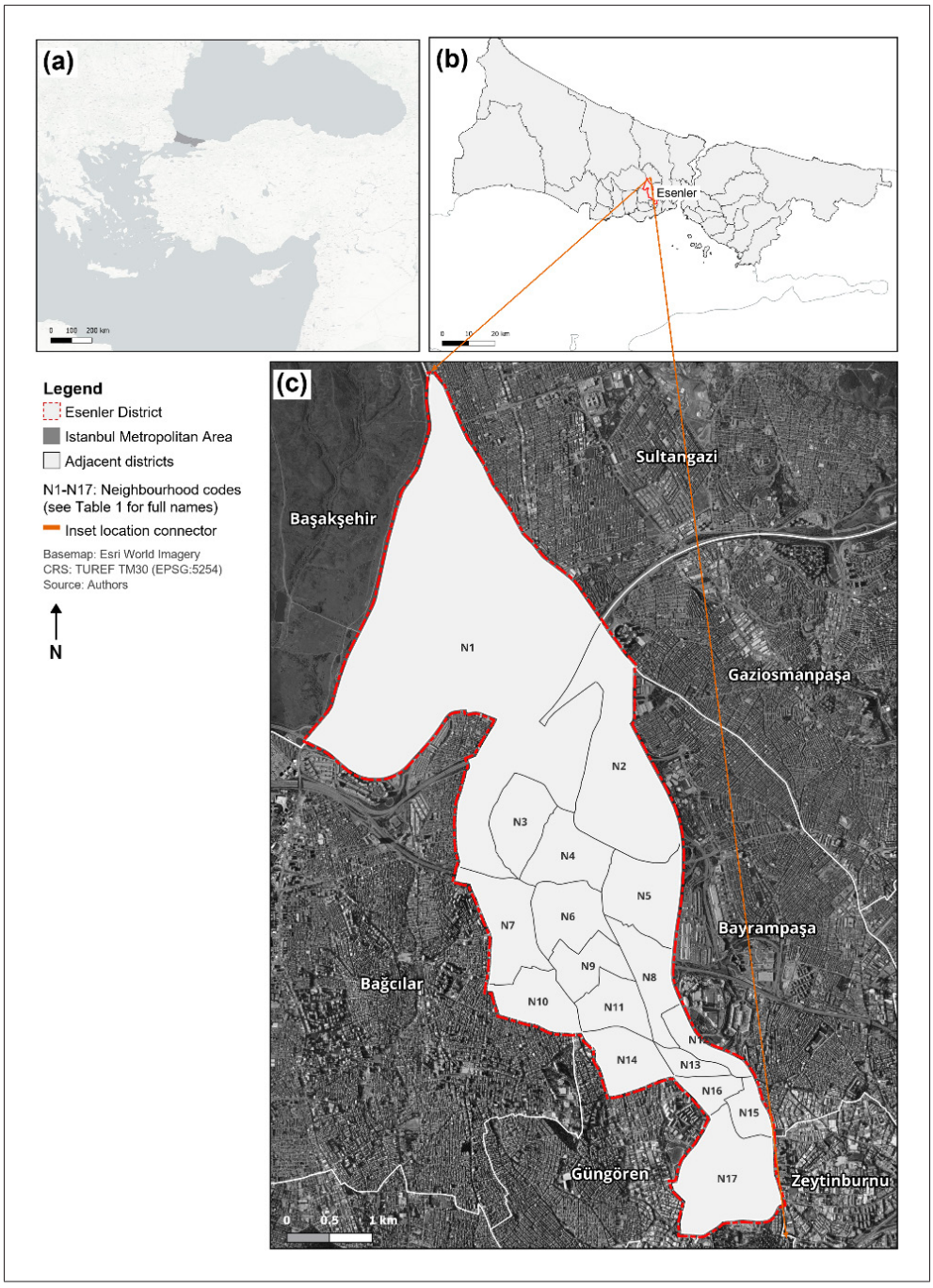

Figure 1. Study area: **(a)** location of Istanbul within Türkiye; **(b)** Esenler district (red dashed boundary) within the Istanbul Metropolitan Area; **(c)** Esenler neighbourhoods (N1–N17) with adjacent districts, overlaid on Esri World Imagery satellite basemap. Neighbourhood codes correspond to Table 1. Coordinate reference system: TUREF TM30 (EPSG:5254). (Designs by Authors).

Meteorologically, Esenler experiences a Mediterranean climate (Csa), characterized by hot, dry summers and mild, wet winters. The warm season spans from June to September, with average daily high temperatures exceeding 25°C and August representing the hottest month, with average highs around 28°C and lows near 18°C (WeatherSpark, 2025; Climate Data, 2025). Extreme events pose significant risks: a study analyzing heatwaves in Istanbul between 2013 and 2017 found that three major heatwaves resulted in 419 excess deaths over 23 days, underlining the vulnerability of urban populations (Can et al., 2019). At the national scale, Turkish provinces have experienced measurable increases

Table 1. Neighborhood-level socio-demographic characteristics of Esenler.

Neighborhood	ID	Population	Population Density (persons/ha)	% Children <5	% Elderly ≥65	% Female population	Illiteracy Rate (%)	Basic Education (%)	Higher Education (%)	Per-capita Income (TL/person/month)
Oruçreis	N1	34657	39.45	6.7	4.7	48.78	2.5	82.0	9.9	14.312
15 Temmuz	N2	8174	471.7	4.92	3.84	37.65	0.24	34.7	2.85	17.713
Turgut Reis	N3	43970	750.7	6.3	4.6	49.29	2.1	73.1	9.4	14.516
Havaalanı	N4	33452	541.8	6.82	4.46	49.50	1.33	66.4	13.0	17.335
Kemer	N5	21554	288.3	6.58	5.35	49.28	1.64	70.3	11.0	17.048
Birlik	N6	26216	429.7	6.20	5.43	49.54	1.90	73.0	10.8	16.195
Tuna	N7	31762	435.5	7.2	5.1	48.61	2.5	69.9	8.6	13.290
Fevzi Çakmak	N8	31081	579.7	6.41	5.21	49.44	1.73	69.1	12.6	14.253
Kazım Karabekir	N9	34092	792.4	6.37	5.35	49.50	2.17	70.9	11.1	15.815
Fatih	N10	41515	810.8	6.83	4.69	48.95	2.00	71.3	9.6	14.765
Menderes	N11	30888	687.9	6.01	5.64	49.42	1.82	68.1	11.96	17.219
Yavuz Selim	N12	3517	145.9	6.0	7.8	48.20	1.5	68.4	14.2	16.741
Mimar Sinan	N13	13216	762.5	5.86	8.41	49.76	1.49	65.7	14.8	16.485
Nine Hatun	N14	40028	793.7	6.1	6.0	49.46	2.2	69.7	10.9	16.374
Namık Kemal	N15	15817	671.5	5.98	5.83	47.90	1.75	68.7	11.7	17.417
Davutpaşa	N16	15757	754.5	5.48	7.47	49.43	1.67	69.5	12.4	18.717
Çifte Havuzlar	N17	2205	18.7	5.17	7.80	46.96	2.40	67.66	11.30	16.696

in annual mean temperatures, drought frequency, and extreme weather events over the past two decades, with built environment characteristics identified as significant drivers of these changes (Bektaş & Sakarya, 2023).

The temporal scope of this study focuses on summer 2024, with the Landsat 8-derived LST map of 13 August 2024 selected to represent peak summer thermal conditions across Esenler. A single cloud-free image was used to capture spatial variations in surface temperature and identify relative heat-exposure hotspots at the neighborhood scale. This approach is widely applied in urban heat vulnerability studies to assess intra-urban thermal variability and evaluate the socio-environmental drivers of heat risk. Although a single-date analysis cannot capture seasonal or temporal fluctuations in temperature, it provides a consistent snapshot of peak heat conditions and a robust basis for identifying priority areas for localized adaptation strategies.

Methodology/Analytical Framework

Neighborhood-scale heat vulnerability in Esenler was assessed using the IPCC Exposure–Sensitivity–Adaptive Capacity framework. Environmental, socio-demographic, and adaptive capacity indicators were preprocessed in GIS, normalized, and prepared as thematic layers. The composite HVI was first calculated using the EW method to represent neighborhood-level vulnerability. To evaluate the robustness and sensitivity of the results to the weighting choice, EWM was subsequently applied as a robustness check. Following the HVI calculation, the results were mapped in QGIS to identify spatial patterns of vulnerability across neighborhoods. Finally, the HVI results were integrated with Adaptive Capacity classes through an HVI–Adaptive Capacity (HVI–AC) Priority Matrix to classify neighborhoods according to adaptation priority levels and support targeted heat adaptation and mitigation planning (Figure 2).

Indicator selection

The construction of the HVI for Esenler was guided by the IPCC framework, which conceptualizes vulnerability as a function of exposure, sensitivity, and adaptive capacity (IPCC, 2014; IPCC, 2022). Indicator selection was informed by a PRISMA-guided systematic literature review. A search was conducted in the Scopus database using the search string ("Heat Vulnerability Index" OR HVI OR "urban heat vulnerability") AND (exposure OR sensitivity OR "adaptive capacity"). Studies published between 2015 and 2025 were identified and screened according to predefined eligibility criteria. Following the review process, 41 studies were retained and used to identify, evaluate, and justify the

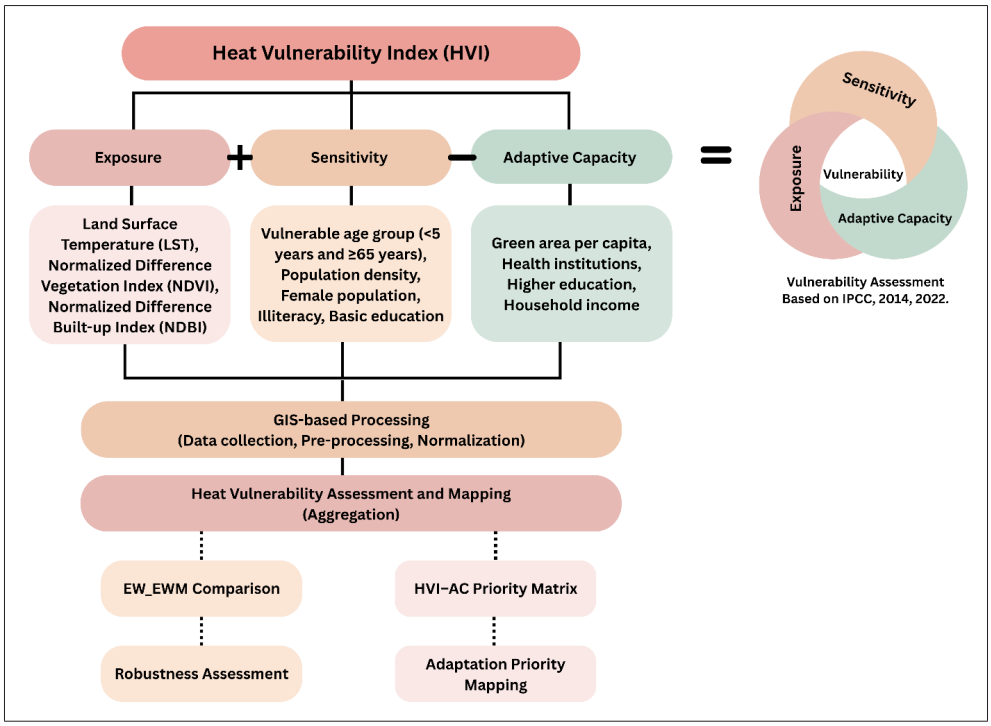

Figure 2. Methodological framework of the study showing the workflow for neighborhood-scale HVI assessment in Esenler (Design by Authors).

indicators included in this research. These studies reveal substantial variation in indicator selection, reflecting differences in local environmental conditions, data availability, and methodological choices. In particular, population density, impervious surfaces, and vegetation cover are inconsistently categorized across studies as exposure, sensitivity, or adaptive capacity, underscoring the flexibility but also the need for contextual tailoring in HVI construction (Chen et al., 2025b; Li et al., 2025; Parker et al., 2025; Cangüzel & Coşkun Hepcan, 2024).

The full list of reviewed studies is presented in Appendix A. Based on methodological precedent and the constraints of neighborhood-scale data availability in Esenler, a set of indicators was selected (Table 2). This framework balances rigor with contextual relevance, ensuring that the HVI reflects environmental heat exposure and socio-demographic factors influencing vulnerability.

Exposure Indicators

Exposure refers to the degree to which Esenler's residents are subjected to intensified thermal stress. In this study, three indicators were adopted, consistent with approaches identified by prior urban heat vulnerability research (Parker et al., 2025; Kim et al., 2023; Zeng et al., 2022):

a. Land Surface Temperature (LST): LST directly reflects surface heat intensity and is widely used as a proxy for localized thermal environments. Higher LST is consistently associated with increased heat exposure and related health risks (Parker et al., 2025; Adnan et al., 2024). Since ground-based meteorological stations in Esenler were not accessible, satellite-derived LST data were employed as a proxy to assess neighborhood-scale heat exposure. While this approach captures spatial variability effectively, it may slightly overestimate temperatures experienced at human height. As highlighted by Parker et al. (2025), LST represents the thermal state of urban surfaces rather than direct air temperatures, and its relationship with surface air temperature can vary depending on season, weather, and urban morphology. Nevertheless, its high spatial resolution provides valuable insights into intra-urban thermal variations (Parker et al., 2025).

b. Normalized Difference Vegetation Index (NDVI): NDVI quantifies vegetation cover, which mitigates surface heat through shading and evapotranspiration. Higher NDVI values indicate greater cooling potential (Zhang et al., 2023).

c. Normalized Difference Built-up Index (NDBI): NDBI measures built-up density and impervious surface cover, both of which increase heat storage and nocturnal warming (Parker et al., 2025).

These indicators are among the most frequently applied in urban heat vulnerability assessments, as documented in the reviewed studies, and they capture the spatial variation of urban morphology and greenery, the two primary drivers

Table 2. Indicators used in constructing the HVI for Esenler, including justification and expected effect on vulnerability.

Dimension	ID	Indicator	Justification	Expected effect on HVI	References	Frequency in literature (%)
Exposure	E-01	Land Surface Temperature (LST)	Proxy for surface heat intensity; widely adopted in neighborhood-scale HVI studies	+	Chen et al. (2025a); Li et al. (2025); Parker et al. (2025); Guo et al. (2024); Kitchley (2024); Fall et al. (2023); Sun et al. (2022)	76%
	E-02	Normalized Difference Vegetation Index (NDVI)	Captures vegetation cover and the cooling effect of greenery	-	Chen et al. (2025b); Parker et al. (2025); Kim et al. (2023); Zeng et al. (2022)	51%
	E-03	Normalized Difference Built-up Index (NDBI)	Reflects urban morphology and impervious surface density influencing heat retention	+	Parker et al. (2025); Adnan et al. (2024); Cangüzel and Coşkun Hepcan (2024); Zeng et al. (2022)	29%
Sensitivity	S-01	% of children (<5 years)	Higher vulnerability to heat-related health risks	+	Li et al. (2025); Li et al. (2024); Guo et al. (2024); Bu et al. (2024); Kamal et al. (2022); Inostroza et al. (2016)	63%
	S-02	% of elderly (≥65 years)	Physiological susceptibility to extreme heat	+	Chen et al. (2025a); Wang et al. (2025); Li et al. (2025); Li et al. (2024); Wang et al. (2024); Guo et al. (2024); Bu et al. (2024); Mallen et al. (2019)	81%
	S-03	% Female population	Women face higher risks of heat-related mortality	+	Kitchley (2024); Wang et al. (2024); Raja et al. (2021); Tran et al. (2020)	17%
	S-04	Population density	Proxy for concentrated human exposure and limited cooling opportunities	+	Chen et al. (2025a); Chen et al. (2025b); Li et al. (2025); Wang et al. (2024); Kitchley (2024); Fall et al. (2023); Salleh et al. (2023); Zuhra et al. (2019)	71%
	S-05	Illiteracy	Low literacy increases vulnerability by limiting awareness of heat risks	+	Kitchley (2024); Raja et al. (2021); Tran et al. (2020)	10%
	S-06	Basic education	Limited formal education reduces coping capacity	+	Li et al. (2025); Hammer et al. (2020); Zhang et al. (2018)	10%
Adaptive Capacity	AC-01	Green area per capita (m^2/person)	Environmental resource mitigating heat stress	-	Chen et al. (2025a); Cangüzel and Coşkun Hepcan (2024); Shartova et al. (2024); Ramsey et al. (2024); Zhang et al. (2019); Weber et al. (2015)	42%
	AC-02	Health institutions	Institutional resource for responding to heat-related health risks	-	Parker et al. (2025); Shartova et al. (2024); Wang et al. (2024); Sianturi et al. (2023); Munoz-Pizza et al. (2023); Singh (2023); Bhattacharjee et al. (2019); Oh et al. (2017)	29%
	AC-03	Higher education	Higher education enhances knowledge and adaptive behaviors	-	Chen et al. (2025b); Jiang (2023)	20%
	AC-04	Household income	Socio-economic vulnerability influencing coping capacity; higher income reduces vulnerability	-	Wang et al. (2025); Chen et al. (2025b); Bu et al. (2024); Yang and Zhao (2023)	20%

of neighborhood-scale heat exposure in Esenler's dense urban fabric.

Sensitivity Indicators

Sensitivity represents the demographic and socio-economic characteristics that influence how severely populations experience heat stress. In this study, six indicators were selected, consistent with patterns identified in the reviewed studies and supported by prior evidence linking them to heat-related morbidity and mortality (Chen et al., 2025b; Li et al., 2025; Fall et al., 2023):

a. Children under 5 years (%) and the Elderly population ≥65 years (%): Frequent and intense heatwaves pose serious health risks to residents, particularly vulnerable groups such as young children and the elderly (Li et al., 2025).

b. Gender (female population %): Gender is an important indicator of heat sensitivity. Physiological differences and health status can increase women's vulnerability, particularly during pregnancy or menopause (Raja et al., 2021). In Istanbul, women have shown higher risks of heat-related mortality (Yılmaz et al., 2024). Similar findings were reported in a Czech study, which observed higher excess female mortality during heat waves (Vésier & Urban, 2023). Zhou et al. (2025b) also found that females are at greater cardiovascular risk under extreme heat.

c. Population density: Higher population density intensifies anthropogenic heat emissions, since densely built urban areas trap heat, leading to elevated temperatures relative to nearby rural zones (Chen et al., 2025a). Esenler is characterized by a compact urban form and high residential density, conditions that contribute to elevated urban heat accumulation and increased heat exposure (Sari et al., 2022).

d. Illiteracy rate and basic education attainment: Lower literacy and education levels limit awareness of heat risks and adaptive behaviors, increasing vulnerability. They are also associated with higher heat-related mortality, likely due to limited economic resources and reduced adaptive capacity (Kitchley, 2024; Li et al., 2024; Hammer et al., 2020).

Adaptive Capacity Indicators

Adaptive capacity is conceptualized in this study as the socio-economic and infrastructural resources that enable communities to cope with heat-related risks. Adaptive capacity reflects the resources and infrastructure that enable communities to cope with or reduce heat exposure. Four indicators were selected, building on previous HVI studies (Cresswell et al., 2023; Guo et al., 2024; Kitchley, 2024; Chen et al., 2025a):

a. Green area per capita (m^2/person): Availability of green space mitigates urban heat stress and provides thermal comfort (Chen et al., 2025a).

b. Health institutions: Access to healthcare facilities strengthens institutional capacity to respond to heat-related health risks (Wang et al., 2025; Guo et al., 2024).

c. Higher education attainment: Higher education levels enhance risk awareness, access to information, and adaptive behavior (Chen et al., 2025a).

d. Household income: Higher income enhances the ability to afford adaptive measures (e.g., cooling devices, quality housing), thereby reducing vulnerability (Wang et al., 2025). In Esenler, where 75% of the population belongs to the low-income group, limited financial capacity increases residents' sensitivity to heat and constrains adaptive options (Sari et al., 2022).

Health-related indicators (e.g., chronic disease prevalence) and housing indicators (e.g., building quality, household crowding) were excluded due to the lack of reliable neighborhood-scale data. While housing quality and health status could further refine sensitivity, their absence may slightly underestimate vulnerability in low-income neighborhoods, an acknowledged limitation for future data integration. Nevertheless, the selected indicators capture the most relevant adaptive resources in Esenler's context. This tailored framework reflects both established practices in HVI construction and the specific socio-environmental conditions of Esenler, ensuring methodological robustness and practical relevance for urban heat mitigation planning.

Data collection and processing

Data for the HVI were collected from multiple spatial, environmental, and socio-demographic sources. Table 3 summarizes all indicators, including source, year, expected effect on vulnerability, normalization approach, spatial resolution/unit, and processing notes.

LST served as the principal indicator of heat exposure. Daytime LST values were derived from the Landsat 8 OLI/TIRS Collection 2 Level 2 Surface Reflectance product (Scene ID: LC08_L2SP_180031_20240813_20240822_02_T1), which provides a surface temperature band (TIRS Band 10; ST_B10) from the Thermal Infrared Sensor (Zhang et al., 2023; Méndez-Lázaro et al., 2018). The dataset corresponds to Path 180/Row 031 under the Landsat World Reference System and was acquired on 13 August 2024 at 09:51 UTC (12:51 local time in Türkiye). It was preprocessed by the USGS at 30-m spatial resolution and used to generate a cloud-free scene representing peak summer heat in Esenler. LST captures intra-urban variations in surface heating and is widely used in neighborhood-scale heat vulnerability assessments (Parker et al., 2025; Guo et al., 2024). The raw satellite data were converted to degrees Celsius using the calibration metadata provided with the product according to:

Table 3. Data sources and processing details for HVI indicators.

ID	Indicator	Source / Year	Normalization	Spatial Resolution/Unit	Notes / Processing
E-01	LST	Landsat 8 OLI/TIRS, 13 August 2024	Min–max, positive	30 m	Extracted from the ST_B10 band, DN → °C
E-02	NDVI	Landsat 8 OLI/TIRS, 13 August 2024	Min–max, inversely aligned	30 m	Calculated from NIR and Red bands
E-03	NDBI	Landsat 8 OLI/TIRS, 13 August 2024	Min–max, positive	30 m	Calculated from SWIR & NIR bands
S-01	% of children (<5 years)	Endeksa, 2025	Min–max, positive	Neighborhood	Census-based, aggregated
S-02	% of elderly (≥65 years)	Endeksa, 2025	Min–max, positive	Neighborhood	Census-based, aggregated
S-03	Female population	Endeksa, 2025	Min–max, positive	Neighborhood	% of total population
S-04	Population density	TÜİK, 2023	Min–max, positive	Neighborhood	Population per neighborhood area
S-05	Illiteracy	Endeksa, 2025	Min–max, positive	Neighborhood	% non-literate population
S-06	Basic education	Endeksa, 2025	Min–max, positive	Neighborhood	% with only basic education
AC-01	Green area per capita (m^2/person)	YAYSIS, 2024	Min–max, inversely aligned	Neighborhood	Green area/population
AC-02	Health institutions	National Smart City Open Data Platform, 2024	Min–max, inversely aligned	Neighborhood	Health institutions per neighborhood
AC-03	Higher education	Endeksa, 2025	Min–max, inversely aligned	Neighborhood	% of population with university education
AC-04	Household income	Endeksa, 2025	Min–max, inversely aligned	Neighborhood	Median household income per neighborhood

$$LST(^{\circ}C) = (DN \times 0.00341802 + 149.0) - 273.15 \quad (1)$$

where DN represents the digital number of Landsat 8 Band 10 thermal pixels, and the rescaling coefficients (0.00341802 and 149.0) were obtained from the Landsat Collection 2 Level-2 metadata (MTL) file provided by the USGS.

NDVI was calculated from OLI Bands 5 (NIR) and 4 (Red) to represent vegetation cover and its cooling potential (Kitchley, 2024; Kim et al., 2023). NDVI values theoretically range from −1 to +1, with higher values indicating greater vegetation density and associated cooling effects. NDBI was derived from OLI Bands 6 (SWIR1) and 5 (NIR) from the same Landsat 8 scene to quantify impervious surfaces and urban density, reflecting heat retention potential in built-up areas (Zhang et al., 2023). Higher NDBI values correspond to more urbanized areas, typically associated with higher surface temperatures.

$$\mathrm{NDVI} = \frac{NIR-Red}{NIR+Red} \quad (2)$$

$$NDBI = \frac{SWIR-NIR}{SWIR+NIR} \quad (3)$$

Data on population density were obtained from TÜİK (2023). Data on age structure (% children under 5, % elderly ≥65), educational attainment (basic education), literacy, and female population proportion were obtained from Endeksa (2025). Green area per capita was calculated by dividing the total green space area by the neighborhood population. Health institutions were represented by the number of hospitals, clinics, and healthcare centers per neighborhood. Data on urban green spaces were obtained from the Istanbul Green Area Management System (YAYSIS) maintained by the Istanbul Metropolitan Municipality (2024). Only publicly accessible green spaces, such as parks and recreational areas, were included in the analysis, while cemeteries, roadside vegetation, and median strips (refüj) were excluded to better represent usable community greenery. Health-service locations were retrieved from the National Smart City Open Data Platform (2024), which includes both public and private health facilities as well as community-based clinics. For consistency, the metric followed the World Health Organization's Health System Strengthening Handbook (2010) definition of static health facilities, adapted to represent the number of health institutions per 1,000 residents. This provides a standardized indicator of healthcare accessibility and social infrastructure relevant to neighborhood-level adaptive capacity. Although both datasets represent key elements of neighborhood resilience, a spatial accessibility analysis was also conducted to assess

the walkable reach of these facilities. Isochrone buffers of 500 metres for green spaces (WHO Regional Office for Europe, 2016) and 400 metres for healthcare facilities (Alshuwaikhat & Aina, 2006) were generated in QGIS. Higher education attainment was measured as the percentage of the population with university-level education, and household income per capita was included as an adaptive capacity indicator, both based on data from Endeksa (2025).

All spatial datasets were standardized before analysis to ensure spatial and thematic consistency. Raster and vector layers were processed in QGIS 3.34.15 "Prizren," projected to the Turkish National Coordinate Reference System (TUREF / TM30, EPSG: 5254). All indicators were normalized to a 0–1 scale using the min–max normalization method, allowing comparability across differing units and value ranges. Within the exposure and sensitivity dimensions, indicators where higher values represent lower vulnerability, namely NDVI, were inverted so that higher normalized values correspond to higher vulnerability. The four adaptive capacity indicators (green area per capita, health institutions, higher education attainment, and household income) were deliberately retained in their natural direction, such that higher normalized values represent greater adaptive capacity. Interpretive consistency in the composite index is instead achieved through the HVI formula (Section 3.4), in which the adaptive capacity component is subtracted: neighbourhoods with greater capacity thereby obtain lower vulnerability scores. The resulting standardized dataset provided a harmonized spatial foundation for subsequent weighting (Section 2.2.3) and spatial integration to generate neighborhood-level heat vulnerability maps (Section 2.2.4).

Weighting and aggregation of indicators

Heat-vulnerability studies employ various weighting approaches depending on study design, indicator set, and data availability. In our review of 41 urban heat vulnerability studies, weighting approaches were distributed as follows: PCA (31.7%), equal weighting (24.4%), entropy weighting (9.8%), expert-based weighting (9.8%), machine learning (2.4%), factor analysis (4.9%), and combination approaches (17.1%). This pattern is consistent with previous reviews, which also found that statistical approaches (e.g., PCA) and equal weighting are the most commonly used methods for indicator aggregation (Cheng et al., 2021; Li et al., 2022). Although PCA is commonly used in HVI research (Parker et al., 2025; Adnan et al., 2024; Kitchley, 2024), it was not suitable here because the Esenler dataset includes only 13 indicators across 17 neighborhoods, yielding approximately 1.3 cases per indicator, well below the recommended 5–10 cases for stable component loadings (Tabachnick & Fidell, 2013; Mundfrom et al., 2005). Moreover, rigorous evaluation of weighting choices is often overlooked in heat-vulnerability research; nearly two-thirds of current HVI studies lack rigorous testing against observed outcomes (Li et al., 2025), underscoring the need for more transparent and replicable evaluation frameworks. Accordingly, the Equal Weighting (EW) approach was adopted as the primary method for HVI construction, assigning identical importance to all indicators to ensure transparency and interpretability. The EWM was subsequently applied as a robustness check by recalculating the exposure, sensitivity, and adaptive capacity indices and the resulting HVI, using entropy-derived indicator weights. This parallel application enabled the assessment of how different weighting schemes influence neighborhood-level vulnerability patterns without altering the overall analytical framework of the study.

Equal Weighting

All indicators were assigned equal importance. After normalization, values were aggregated using a simple arithmetic mean to produce three intermediate component scores for each neighborhood: Exposure (EXP_n), Sensitivity ($SENS_n$), and Adaptive Capacity ($ADAP_n$).

Exposure, Sensitivity, and Adaptive Capacity each contributed one-third to the composite HVI. This approach is well-suited to small-sample, neighborhood-scale studies, improving transparency and avoiding methodological instability. However, it involves trade-offs: equal weighting may mask the disproportionately strong influence of certain socio-economic indicators, such as household income or education, which are known to drive vulnerability in Esenler.

Entropy Weighting Method (EWM)

To complement equal weighting and incorporate the intrinsic variation of each indicator, the Entropy Weighting Method was applied. EWM assigns weights based on the distribution of each indicator across neighborhoods: indicators with higher variability are given greater influence in the aggregation, reflecting their relative contribution to overall heat vulnerability. This method is widely recognized as an objective approach for assessing value dispersion in decision-making, as it minimizes human bias and enhances the objectivity of composite evaluations compared to subjective weighting techniques (Guo et al., 2024; Yang & Zhao, 2023). This makes it particularly suitable for small, data-limited urban studies such as Esenler. The procedure for the calculations is outlined below (Guo et al., 2024; Yang & Zhao, 2023):

An initial index matrix $X = [x_{ij}]$ was created, where $i = 1, \ldots, n$ represents the samples (e.g., neighborhoods) and $j = 1, \ldots, m$ represents the indicators. To remove dimensional inconsistencies, the matrix was normalized.

For positive indicators (larger values indicate higher vulnerability), the normalized value y_{ij} was calculated as shown in Equation (4):

$$y_{ij} = \frac{X_{ij} - \min(X_j)}{max(X_j) - \min(X_j)} \quad (4)$$

For negative indicators (smaller values indicate higher vulnerability), the normalized value y_{ij} was calculated as shown in Equation (5):

$$y_{ij} = \frac{max(X_j) - X_{ij}}{max(X_j) - \min(X_j)} \quad (5)$$

The proportion of the *j*-th indicator for the *i*-th sample was calculated using Equation (6):

$$p_{ij} = \frac{y_{ij}}{\sum_{i=1}^{n} y_{ij}} \quad (6)$$

The information entropy of each indicator was then computed using Equation (7):

$$H_j = -k \sum_{i=1}^{n} p_{ij} \ln(p_{ij}),\ k = \frac{1}{ln(n)} \quad (7)$$

The redundancy (degree of information) for each indicator was calculated as shown in Equation (8):

$$d_j = 1 - H_j \quad (8)$$

The weight of each indicator was obtained using Equation (9):

$$w_j = \frac{d_j}{\sum_{i=1}^{m} d_j} \quad (9)$$

This procedure ensures that indicators with greater variability across neighborhoods contribute more to the overall heat vulnerability index. All calculations were performed in Excel using these formulas. In this study, the Equal Weighting method was used to calculate the Exposure, Sensitivity, and Adaptive Capacity indices and to construct the final HVI. The Entropy Weighting Method was applied separately to the same set of indicators to generate an alternative HVI as a robustness check. Therefore, the entropy-derived weights were not used in the calculation of the component indices reported in the main analysis.

Mapping and Spatial Analysis

Following indicator weighting and aggregation, spatial integration was performed in QGIS to visualize the neighborhood-level HVI across Esenler. Raster exposure layers (LST, NDVI, NDBI; 30 m) were summarized to neighborhoods via Zonal Statistics (mean) and integrated with vector socio-demographic and adaptive-capacity indicators in QGIS 3.34. The resulting Equal-weighted HVI map illustrates the spatial distribution of heat vulnerability across Esenler District. To evaluate the robustness of the results, an additional set of HVI values was generated using the Entropy Weighting Method. Statistical agreement metrics, including mean difference, standard deviation of differences, and the Pearson correlation coefficient, were calculated to quantify the agreement between the two methods. This comparison enabled the evaluation of how weighting approaches influence vulnerability outcomes and ensured consistency in the identified high-risk neighborhoods.

Heat Vulnerability–Adaptive Capacity Priority Matrix

To support climate adaptation planning, neighborhoods were prioritized through the combined assessment of the Heat Vulnerability Index (HVI) and Adaptive Capacity (AC). This approach follows vulnerability assessment frameworks that emphasize the interaction between vulnerability and adaptive capacity in determining adaptation needs and intervention priorities (IPCC, 2022; Inostroza et al., 2016). The prioritization framework was designed to identify neighborhoods requiring different levels of intervention according to both their heat vulnerability and their capacity to respond to climate-related risks.

Priority levels were assigned using a decision matrix that integrated neighborhood-level HVI scores with AC classes. The HVI results were first classified into three vulnerability categories (low, medium, and high) using the Natural Breaks (Jenks) classification method, and these classes were subsequently combined with adaptive capacity categories to define adaptation priorities. The matrix generated five priority categories representing different levels of adaptation urgency. Priority 1 corresponds to neighborhoods characterized by high vulnerability and low adaptive capacity, indicating the greatest need for immediate intervention. Priority 2 and Priority 3 represent neighborhoods with high vulnerability but varying levels of adaptive capacity, requiring short-term interventions or continuous monitoring. Priority 4 corresponds to areas with relatively low vulnerability and higher adaptive capacity, while Priority 5 represents neighborhoods with the lowest vulnerability and highest adaptive capacity, where resilience maintenance and periodic monitoring are considered sufficient. The resulting priority categories were subsequently mapped to visualize the spatial distribution of adaptation priorities across Esenler District.

RESULTS

Before integrating exposure, sensitivity, and adaptive capacity into a composite HVI, the individual components were examined to explore their spatial variability and underlying drivers across the Esenler District. The analysis highlights substantial variability in thermal, demographic, and socio-economic conditions, revealing patterns that shape neighborhood-level vulnerability to heat.

Exposure Index

Neighborhood-level analysis of LST, NDVI, and NDBI revealed distinct spatial heterogeneity across Esenler District (Table 4). Mean LST values ranged from 42.39°C in N1 to

45.92°C in N9, indicating a temperature difference of more than 3 °C between the coolest and hottest neighborhoods. NDVI values varied between 0.05 and 0.17, while NDBI ranged from -0.04 to 0.08. Higher LST values corresponded with lower NDVI and higher NDBI values; for instance, N9 recorded an average LST of 45.92 °C with NDVI = 0.05 and NDBI = 0.06. Conversely, N1, with NDVI = 0.15 and NDBI ≈ 0.00, exhibited relatively lower surface temperatures. Maps of the individual exposure indicators (LST, NDVI, and NDBI) are provided in Appendix B.

The spatial distribution of the exposure index derived using the Equal Weighting approach (Figure 3) further visualizes this relationship, forming a clear gradient from low to high exposure across neighborhoods. Lighter yellow areas (index ≤ 0.25) represent zones with lower heat exposure, while dark red tones (index > 0.74) denote highly exposed regions. The central and northwestern neighborhoods exhibit the most intense exposure levels, corresponding to high built-up density and limited green cover. In contrast, peripheral zones such as N1 and N17 display relatively moderate to low exposure levels, where greater vegetation coverage contributes to local cooling effects. This spatial gradient provides a visual confirmation of how land surface composition and vegetation patterns shape the microclimatic variability across Esenler.

Sensitivity Index

Socio-demographic indicators used to assess sensitivity show substantial variability among neighborhoods (Table 5). Population density averages 516 persons/ha (SD = 268), reflecting the district's compact urban form, which can intensify exposure to heat. Vulnerable age groups constitute a moderate share of the population: children account for 6.17% and the elderly for 5.74%. The proportion of women is relatively balanced at 47.84%, while educational attainment levels suggest limited adaptive awareness: 1.77% of residents are illiterate, and 67.11% have only a basic education.

The spatial distribution of the sensitivity index (Figure 4) reveals a pronounced north–south gradient across Esenler. Neighborhood N2 shows the lowest sensitivity (index ≤ 0.22), while N9, N10, N13, and N14 display the highest sensitivity values (index ≥ 0.61). The spatial clustering of high sensitivity in the central and southern neighborhoods corresponds to densely populated areas with lower education levels, as detailed in Table 1.

Adaptive Capacity Index

Indicators of adaptive capacity reflect socio-economic and infrastructural resources available to mitigate heat-related risks (Table 6). The mean household income is 16.07 thousand TRY, ranging from 13.29 to 18.71 thousand TRY, re-

Table 4. Neighborhood-level exposure indicators in Esenler (LST, NDVI, NDBI).

Neighbourhoods	LST (Min)	LST (Max)	LST (Mean)	LST (SD)	NDVI (Min)	NDVI (Max)	NDVI (Mean)	NDVI (SD)	NDBI (Min)	NDBI (Max)	NDBI (Mean)	NDBI (SD)
N1	37.42	48.32	42.39	1.91	-0.0198	0.3869	0.15	0.07	-0.2066	0.1333	0.002	0.05
N2	37.72	45.7	42.56	1.36	-0.0059	0.3864	0.11	0.08	-0.2307	0.1767	-0.01	0.05
N3	42.06	48.08	45.84	1.01	0.0184	0.1523	0.05	0.01	-0.0711	0.1341	0.06	0.03
N4	39.37	46.84	44.28	1.76	0.007	0.3697	0.07	0.05	-0.1836	0.1266	0.02	0.05
N5	39.75	48.17	44.49	1.7	0.0255	0.4525	0.11	0.07	-0.1891	0.1322	0.008	0.06
N6	40.96	47.86	44.99	1.51	0.0074	0.3862	0.09	0.06	-0.1714	0.1277	0.02	0.06
N7	41.52	47.99	44.84	1.26	-0.0068	0.3608	0.09	0.07	-0.1702	0.1801	0.02	0.07
N8	40.21	46.7	44.43	1.28	0.0024	0.3948	0.09	0.07	-0.1672	0.1642	0.02	0.07
N9	43.98	48.33	45.92	0.76	-0.0068	0.2492	0.05	0.02	-0.1485	0.1447	0.06	0.04
N10	43.92	47.99	45.52	0.76	0.0121	0.2378	0.05	0.02	-0.0897	0.1471	0.06	0.03
N11	42.09	47.04	44.92	1.02	0.0023	0.2906	0.06	0.03	-0.1256	0.1713	0.05	0.04
N12	42.88	47.62	45.05	1.11	-0.0081	0.2287	0.06	0.04	-0.1135	0.1187	0.01	0.04
N13	42.96	45.88	44.11	0.47	0.0243	0.1011	0.05	0.01	-0.0084	0.1454	0.08	0.03
N14	42.63	46.73	45.05	0.73	0.0178	0.2212	0.05	0.02	-0.0944	0.1903	0.07	0.03
N15	43.71	46.19	45.27	0.43	-0.0012	0.2387	0.07	0.03	-0.0973	0.1455	0.05	0.04
N16	43.19	45.89	44.68	0.49	0.0229	0.2821	0.06	0.03	-0.1143	0.1481	0.06	0.04
N17	37.9	45.98	42.75	1.8	-0.0153	0.4018	0.17	0.08	-0.226	0.179	-0.04	0.06

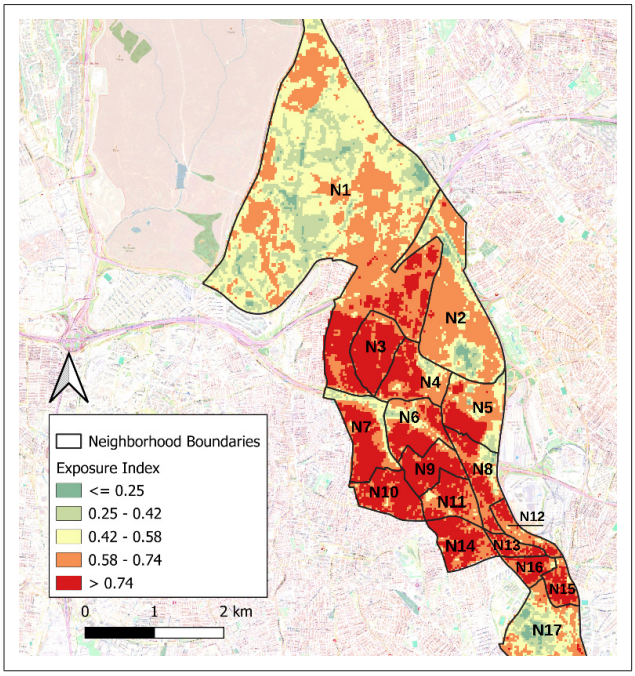

Figure 3. Spatial distribution of exposure index across neighborhoods in Esenler District, integrating LST, NDVI, and NDBI to illustrate variations in thermal stress (Design by Authors).

vealing income disparities across neighborhoods. Green space availability is notably limited, averaging 3.50 m²/person (SD = 5.45), with several neighborhoods containing almost no vegetated areas. Health infrastructure accessibility is also low, with an average of 0.12 health institutions per 1,000 people, suggesting limited service capacity. Higher education levels range from 2.85% to 14.8%, averaging 10.72%.

Substantial variation is also evident in the distribution of environmental and infrastructural resources across neighborhoods. While N2 and N17 exhibit comparatively higher green area per capita (22.84 m² and 5.9 m² per person, respectively), densely populated neighborhoods such as N9, N10, N14, and N16 possess less than 0.2 m² per person, indicating severe shortages of cooling and recreational spaces. Healthcare infrastructure also varies widely, from neighborhoods such as N17, N6, and N8 (0.45, 0.19, and 0.12 facilities per 1,000 people, respectively) to those lacking any institutions, such as N2 and N12 (Table 7). These disparities highlight unequal access to adaptive resources and support services that may constrain the capacity of some neighborhoods to cope with heat-related risks. The complementary buffer analysis further indicated generally good walkable accessibility across neighborhoods, suggesting that while per-capita variation reflects structural provision within administrative boundaries, actual use patterns may extend beyond them. Together, these metrics provide a more comprehensive representation of adaptive capacity by capturing both the structural availability and functional accessibility of key urban infrastructure that supports resilience to heat stress.

The adaptive capacity index map (Figure 5) illustrates these differences spatially, showing that neighborhoods N1, N3, N7, and N10 have the lowest capacity (index = 0.17–0.26), while N17 exhibits the highest (0.64). Lower-income areas with limited green space and healthcare access correspond with reduced adaptive capacity.

Table 5. Sensitivity indicators describing socio-demographic characteristics of the district.

Indicator	Min	Max	Mean	SD
Population Density	18.7	810.8	516.01	268
% Children	4.92	7.20	6.17	0.59
% Elderly	3.84	8.41	5.74	1.33
% Female	37.65	49.76	47.84	2.84
Illiteracy	0.24	2.5	1.77	0.53
Basic Education	34.7	82	67.11	9.34

Equal-weighted HVI

Following normalization and alignment of all indicators, the composite HVI was computed using the Equal Weighting Method, where exposure, sensitivity, and adaptive capacity contributed equally to the final score:

$$HVI = \frac{Exposure + Sensitivity - Adaptive\ Capacity}{3}$$

Raster-based exposure data were summarized using zonal statistics to ensure comparability with vector-based socio-economic indicators. Resulting HVI values range from 0.068 to 0.414, reflecting considerable intra-district variation (Figure 6). Neighborhoods N2 and N17 recorded the lowest vulnerability (0.068–0.21), whereas N3, N7, N9, N10, and N14 showed the highest (0.35–0.41). Cross-referencing Table 1 and component indices reveals that these highly vulnerable neighborhoods combine multiple risk factors: N9 and N10, for instance, exhibit the highest population densities (≈790–810 persons/ha) and lower high-

Table 6. Adaptive capacity indicators describing economic, infrastructural, and educational conditions across neighborhoods.

Indicator	Min	Max	Mean	SD
Higher Education	2.85	14.8	10.72	2.65
Household Income	13.29	18.71	16.07	1.46
Green area per capita (m²/person)	0	22.84	3.50	5.45
Health Institutions per 1,000 people	0	0.45	0.12	0.10

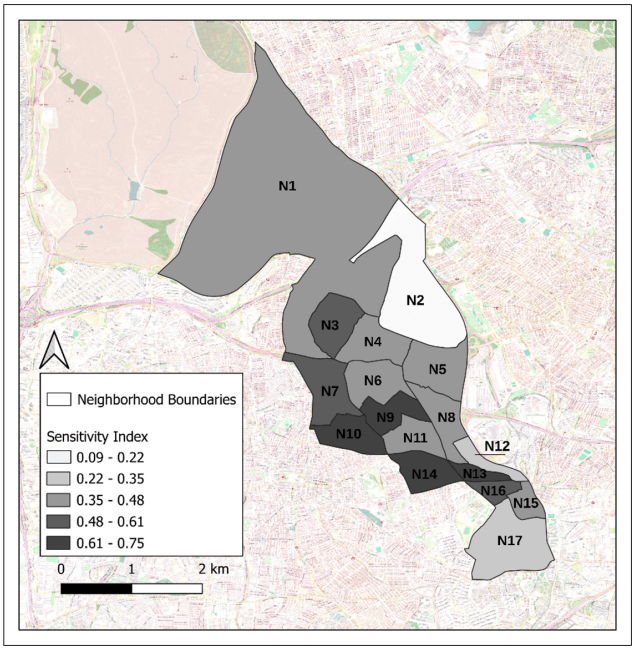

Figure 4. Spatial distribution of the sensitivity index across Esenler District, highlighting neighborhoods with higher demographic and educational vulnerability (Design by Authors).

er-education rates (≈9–11%), coupled with limited green space and higher mean LST values (≈45.5–45.9 °C). Conversely, N2 and N17, which recorded the lowest vulnerability, have lower population densities and relatively higher income levels, alongside cooler surface temperatures and greater vegetation coverage.

These neighborhoods combine high exposure and demographic sensitivity with relatively low adaptive capacity. The equal-weighted HVI map (Figure 6) provides a baseline representation of heat vulnerability across Esenler, clearly differentiating low-, medium-, and high-risk zones. These vulnerability classes were derived using the Natural Breaks (Jenks) classification method, which identifies statistically meaningful thresholds based on the distribution of HVI values. Although this approach assumes equal contribution of each component, it offers a transparent, balanced measure that facilitates comparison between neighborhoods.

Robustness Assessment

To evaluate the reliability of the HVI, the Equal-weighted results were compared with those derived from the Entropy Weighting Method, which objectively determines indicator importance based on data variability. Table 8 presents neighborhood-level HVI values for both methods, along with differences and standardized deviations. Most neighborhoods exhibited small deviations ($|\Delta HVI| < 0.05$), indicating strong consistency between methods. Larger deviations appeared in a few central neighborhoods, notably N4, N7, and N10, where entropy weighting slightly increased vulnerability scores due to greater dispersion among indicators.

Table 7. Neighborhood-level environmental and infrastructural indicators of Esenler.

Neighborhood	ID	Green Area (m²)	Green Area per Capita (m²/person)	Health Institutions	Health Facilities per 1,000 People
Oruçreis	N1	17,437	0.50	3	0.086
15 Temmuz	N2	186,760	22.84	0	0
Turgut Reis	N3	8,574	0.19	4	0.09
Havaalanı	N4	54,671	1.63	4	0.11
Kemer	N5	44,949	2.08	1	0.046
Birlik	N6	41,282	1.57	5	0.19
Tuna	N7	62,544	1.96	2	0.062
Fevzi Çakmak	N8	22,035	0.70	4	0.12
Kazım Karabekir	N9	6,028	0.17	4	0.11
Fatih	N10	2,609	0.06	4	0.096
Menderes	N11	14,845	0.48	4	0.12
Yavuz Selim	N12	14,723	4.18	0	0
Mimar Sinan	N13	5,601	0.42	2	0.15
Nine Hatun	N14	6,448	0.16	4	0.099
Namık Kemal	N15	15,957	1.00	1	0.063
Davutpaşa	N16	0	0	1	0.063
Çifte Havuzlar	N17	13,027	5.90	1	0.45

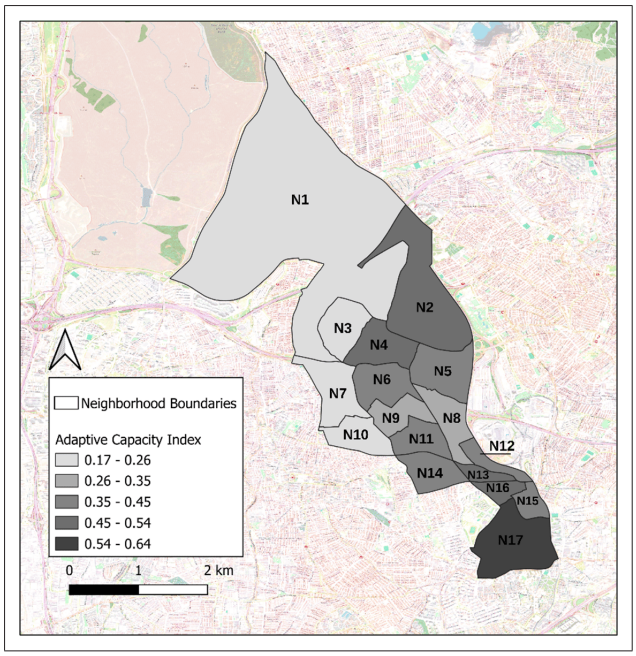

Figure 5. Spatial distribution of the adaptive capacity index across Esenler District, showing higher resilience in darker areas and lower capacity in lighter areas (Design by Authors).

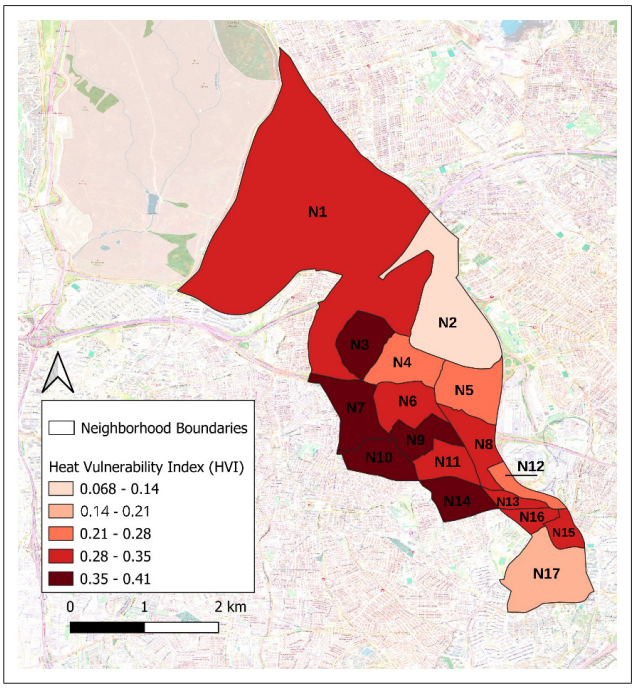

Figure 6. Spatial distribution of the Heat Vulnerability Index (HVI) across Esenler District, illustrating neighborhood-level variations in vulnerability based on exposure, sensitivity, and adaptive capacity indicators (Design by Authors).

Summary statistics (Table 9) show a mean difference of 0.017, a standard deviation of 0.049, and a Pearson correlation coefficient of r = 0.94 ($p<0.001$), confirming strong statistical agreement between the two weighting approaches. This high correlation demonstrates that the equal-weighted HVI reliably represents neighborhood-level heat vulnerability while

Table 8. Validation statistics indicating consistency and reliability between Equal- and Entropy-weighted HVI results.

Neighborhood	Equal-weighted HVI	Entropy-weighted HVI	Difference (Entropy – Equal)	Standardized Deviation (SD)
N1	0.599	0.594	-0.005	-0.022
N2	0.151	0.216	0.065	0.048
N3	0.689	0.696	0.007	-0.010
N4	0.515	0.601	0.086	0.069
N5	0.574	0.582	0.008	-0.009
N6	0.584	0.575	-0.009	-0.026
N7	0.690	0.770	0.080	0.063
N8	0.604	0.624	0.020	0.003
N9	0.670	0.694	0.024	0.007
N10	0.685	0.775	0.090	0.073
N11	0.583	0.585	0.002	-0.015
N12	0.525	0.547	0.022	0.005
N13	0.589	0.627	0.038	0.021
N14	0.646	0.661	0.015	-0.002
N15	0.602	0.584	-0.018	-0.035
N16	0.573	0.548	-0.025	-0.042
N17	0.428	0.315	-0.113	-0.130

Table 9. Summary statistics and validation metrics demonstrating the consistency and reliability of Equal- and Entropy-weighted HVI results across neighborhoods in Esenler District.

Metric	Formula	Value
Mean Difference	$\bar{d}_{=} \frac{\sum(HVI_{entropy} - HVI_{equal})}{n}$	0.017
Standard Deviation of Differences	$s = \sqrt{\frac{\sum(d_i - \bar{d})^2}{n-1}}$	0.049
Mean Absolute Difference (MAD)	$MAD = \frac{\sum(HVI_{entropy} - HVI_{equal})}{n}$	0.0369
Pearson Correlation Coefficient	$r = \frac{\sum(x_i - \bar{x})(y_i - \bar{y})}{\sqrt{\sum(x_i - \bar{x})^2 \sum(y_i - \bar{y})^2}}$	p <0.001)

maintaining simplicity and transparency. The close spatial correspondence between the two HVI values validates the robustness of the applied framework and supports its use for further spatial and temporal analyses of heat vulnerability.

DISCUSSION

The analysis reveals that Esenler's most densely built and socio-economically disadvantaged neighborhoods exhibit the highest heat vulnerability, whereas areas with greater green space or improved infrastructure display lower vulnerability. In particular, clusters of extreme heat risk were observed in neighborhoods combining high land surface temperatures with low adaptive capacity. This pattern directly addresses Research Question 1, revealing that dense urban form and social disadvantage jointly produce localized hotspots of heat risk, while urban greenery and improved amenities can buffer against extreme heat. Hence, heat vulnerability in Esenler arises from the compound effects of physical exposure and social inequality, highlighting the need for targeted, equity-focused adaptation strategies. This finding is consistent with recent research in Istanbul, which demonstrates that urban heat vulnerability is fundamentally shaped by socio-spatial inequalities, where densely built environments, high population densities, and limited access to cooling resources disproportionately increase heat risk in disadvantaged communities (Okumuş, 2025).

Spatial Patterns of Heat Vulnerability

In Esenler, neighborhoods with the highest Land Surface Temperatures (LSTs), notably N3, N7, N9, and N10, also exhibit limited vegetation and low adaptive capacity. This overlap of dense urban morphology and socio-economic disadvantage illustrates how physical exposure and social sensitivity reinforce each other, creating concentrated heat-risk hotspots. Such an interplay mirrors broader findings from Istanbul (Yılmaz et al., 2024) and other global cities (Li et al., 2025; Parker et al., 2025; Chen et al., 2025b), where the co-occurrence of built-up density, poverty, and insufficient greenery produces clusters of vulnerability. Similar patterns were reported by Inostroza et al. (2016), who found that highly vulnerable neighborhoods in Santiago were characterized by the combined effects of elevated heat exposure, limited green infrastructure, and lower adaptive capacity, reinforcing the importance of assessing vulnerability through the interaction of exposure, sensitivity, and adaptive capacity. Likewise, Okumuş (2025) identified land surface temperature, population density, and building compactness as the dominant drivers of urban heat vulnerability in Istanbul, while green spaces and cooling infrastructure exerted significant mitigating effects. These findings closely align with the spatial patterns observed in Esenler, where neighborhoods characterized by high surface temperatures, dense urban form, and limited adaptive resources exhibited the highest vulnerability levels.

These outcomes align with the IPCC's conceptualization of vulnerability as a product of exposure, sensitivity, and adaptive capacity (IPCC, 2022). In Esenler, limited green space and lower-income levels clearly compound the population's exposure to heat. The district's scarcity of green areas (averaging only ~3.5 m² per person) and its concentrated low-income population jointly reduce resilience, while high population density amplifies anthropogenic heat emissions and inhibits natural ventilation. This spatial inequality in adaptive resources corresponds to the 'green divide' described by Yazar et al. (2023), wherein recent urban regeneration projects have improved microclimates in some zones, while leaving older, denser areas still exposed. Similar disparities were identified by Wang et al. (2025), who showed that urban greening initiatives in New York disproportionately benefited high-income areas, intensifying existing heat vulnerabilities in low-income districts. Macharia and Kiage (2025) similarly found that areas with limited vegetation and high impervious cover in Reno exhibited elevated heat exposure and social vulnerability, reinforcing the global pattern that unequal land-cover dynamics amplify heat risk in marginalized communities.

Overall, our results highlight that urban heat vulnerability is not merely an environmental issue; it reflects the cumulative effects of long-standing unequal planning and socio-economic stratification. The case of Esenler demonstrates how morphological compactness and limited adaptive infrastructure can translate social disadvantage into climatic risk. Addressing heat risk, therefore, requires integrated strategies that span urban planning, public health, and social equity. In other words, efforts must move beyond only physical heat mitigation toward a more systemic approach to building urban resilience.

Influence of Weighting Methods

Addressing Research Question 2, the Comparison between Equal and Entropy weighting methods provides a robustness check of the HVI approach. A high Pearson correlation ($r = 0.94$, $p<0.001$) and a very small mean difference (0.017) between the two sets of results indicate that both weighting schemes yielded nearly identical spatial patterns of vulnerability. This strong agreement suggests that the underlying vulnerability structure in Esenler is robust and not an artifact of any particular weighting choice.

The entropy-weighted HVI did slightly amplify the scores in neighborhoods where indicator variability was greater, particularly in socio-economically diverse areas such as N4 and N10. This reflects the Entropy method's data-driven nature, which assigns greater influence to indicators with higher informational dispersion (Guo et al., 2024). Similar to Chen et al. (2025b), who emphasized the objectivity and data-driven robustness of the Entropy Weight Method in minimizing human bias, our findings confirm that EWM can enhance methodological transparency in vulnerability assessment. Additionally, Li et al. (2025) noted that explicit and statistical weighting approaches often introduce subjectivity or fail to capture non-linear relationships among indicators, underscoring the value of objective, information-based weighting techniques like EWM. Nevertheless, the minimal deviations observed confirm that even a simple equal-weighting scheme provides reliable outcomes for a small-area dataset.

This comparative analysis strengthens confidence in the robustness of the Equal-weighted HVI map. Applying Equal Weighting for its transparency and Entropy Weighting as an objective robustness check provides a useful framework for urban studies in data-limited contexts.The demonstrated stability across weighting schemes establishes a solid methodological foundation for constructing vulnerability indices that can be replicated in other districts of Istanbul or similar urban contexts. Overall, the high consistency between methods validates the robustness of the HVI framework and provides a sound basis for the spatial and planning analyses discussed in the following section.

Implications for Climate Adaptation

Building on the third research question, which examines what specific adaptation interventions the HVI identifies as priorities for different neighborhoods in Esenler, this section translates the spatial findings into actionable urban and policy interventions. The HVI results clearly identify clusters of high vulnerability, particularly in neighborhoods N3, N7, N9, N10, and N14, where limited vegetation and socio-economic disadvantage coincide. These high-risk zones represent priority areas for targeted adaptation efforts.

Applying the HVI–AC Priority Matrix described in Section 2.2.5 resulted in five adaptation priority categories across Esenler (Table 10; Figure 7). Priority 1 areas (N3, N7, and N10) combine the highest HVI values with the lowest adaptive capacity, identifying critical hotspots that demand immediate adaptation measures. Priority 2 neighborhoods (N1, N8, N9, and N14) exhibit high vulnerability coupled with limited adaptive capacity, indicating the need for targeted short-term interventions. Priority 3 neighborhoods represent areas where moderate adaptive capacity partially offsets high vulnerability, suggesting that continuous monitoring and incremental resilience-building measures are appropriate. Priority 4 areas, represented by N2, exhibit relatively low vulnerability and higher adaptive capacity, indicating that existing resilience should be maintained through routine planning measures. Finally, Priority 5 (N17) corresponds to the neighborhood with the lowest vulnerability and highest adaptive capacity, where periodic monitoring and the preservation of existing resilience conditions are considered sufficient.

This prioritization framework provides a spatially explicit basis for staging adaptation actions and allocating resources according to neighborhood-specific needs. Similarly, Okumuş (2025) emphasizes that effective urban heat adaptation requires integrating ecological measures, such as urban greening, with socio-infrastructural interventions, including cooling facilities and public services, highlighting the importance of multi-dimensional and equity-oriented adaptation strategies. By integrating both vulnerability and adaptive capacity, the matrix moves beyond identifying areas of risk and supports the development of targeted and equitable adaptation strategies across Esenler District.

Based on the prioritization outcomes summarized in Table 10, adaptation efforts in Esenler should focus first on the highest-risk neighborhoods (Priority 1–2), while reinforcing resilience in lower-priority zones through sustainable, small-scale interventions. Expanding urban greenery emerges as the most critical and immediate mitigation strategy (Parker et al., 2025; Shartova et al., 2024). Numerous studies have confirmed that increasing urban vegetation can reduce local surface and air temperatures (Parker et al., 2025; Kim et al., 2023). In Esenler, where impervious surfaces account for nearly 80% of total land cover, as reflected by predominantly positive NDBI values (0.02–0.08) across most neighborhoods, large-scale park development is severely constrained. Although a few zones, such as N1 and N17, show slightly negative NDBI values due to institutional or vegetated land, these represent minor exceptions in an otherwise compact urban landscape. Consequently, distributed, small-scale greening emerges as the most feasible and context-sensitive adaptation strategy. In Esenler, the implementation of such measures could be integrated into ongoing municipal urban regeneration, streetscape improvement, and public-space enhancement programs. Given the district's limited availability of vacant land, local authorities may achieve greater benefits by prioritizing street-tree planting, schoolyard

Table 10. Neighborhood Prioritization Matrix for Climate Adaptation in Esenler District.

Neighborhood	HVI	Vulnerability Class	AC Index	AC Class	Priority Level	Interpretation
N1	0.599	High	0.17–0.26	Low	Priority 2	High vulnerability but slightly lower HVI than critical hotspots; very low AC (Short-term intervention)
N2	0.151	Low	0.45–0.54	Medium-High	Priority 4	Low vulnerability and higher AC (Maintain resilience)
N3	0.689	High	0.17–0.26	Low	Priority 1	Highest HVI and lowest AC (Immediate action)
N4	0.515	High	0.45–0.54	Medium-High	Priority 3	High vulnerability but above-average AC (Monitor)
N5	0.574	High	0.35–0.45	Medium	Priority 3	High HVI but moderate AC (Monitor)
N6	0.584	High	0.35–0.45	Medium	Priority 3	Moderate AC balances high vulnerability (Monitor)
N7	0.690	High	0.17–0.26	Low	Priority 1	Extreme vulnerability and lowest AC (Immediate action)
N8	0.604	High	0.26–0.35	Medium-Low	Priority 2	High HVI + limited AC (short-term interventions)
N9	0.670	High	0.26–0.35	Medium-Low	Priority 2	High vulnerability + weak AC (Short-term intervention)
N10	0.685	High	0.17–0.26	Low	Priority 1	High HVI + lowest AC (Immediate action)
N11	0.583	High	0.35–0.45	Medium	Priority 3	High HVI but moderate AC (Monitor)
N12	0.525	High	0.35–0.45	Medium	Priority 3	High HVI but adequate AC (Monitor)
N13	0.589	High	0.45–0.54	Medium-High	Priority 3	High HVI but strong AC (Monitor)
N14	0.646	High	0.35–0.45	Medium	Priority 2	High HVI + moderate AC (Short-term intervention)
N15	0.602	High	0.35–0.45	Medium	Priority 3	High HVI but moderate AC (Monitor)
N16	0.573	High	0.45–0.54	Medium-High	Priority 3	High HVI offset by higher AC (Monitor)
N17	0.428	Medium	0.54–0.64	High	Priority 5	Lowest vulnerability + highest AC (maintain and monitor)

greening, courtyard retrofits, façade greening, and the conversion of underutilized spaces into pocket parks within the neighborhoods identified as Priority 1 and Priority 2. The HVI–Adaptive Capacity Priority Matrix developed in this study can support municipal decision-makers in targeting these interventions where adaptation needs are greatest. Ma et al. (2023) show that small pocket parks (~2,000 m²) cool the air by ~0.4–1.1 °C, extend ~100 m beyond their edges, and boost comfort. A 50% increase in trees cuts daytime PET by ~2.1–2.8 °C. Similarly, Ren et al. (2021) demonstrate that increasing street tree density significantly enhances pedestrian-level comfort, raising canopy cover lowered mean radiant temperature by 13–17 °C and reduced PET by up to 10 °C, confirming the strong cooling benefits of even modest green additions. Complementing these findings, Zhou et al. (2025a) reported that pocket parks ranging from 1,000–9,000 m² in Shanghai decreased air temperature by ~1.2 °C and improved thermal comfort, with greater canopy height and uneven tree distribution amplifying these effects. Unlike Istanbul's lower-density districts, where new urban parks remain feasible, Esenler's adaptation requires micro-scale, embedded greenery integrated into the existing built form. Yılmaz et al. (2024) demonstrated that strategically distributed vegetation can provide significant cooling effects even in areas with limited space. This finding reinforces that context-sensitive and modular greening represents the most practical approach to mitigating urban heat within Esenler's densely built environment.

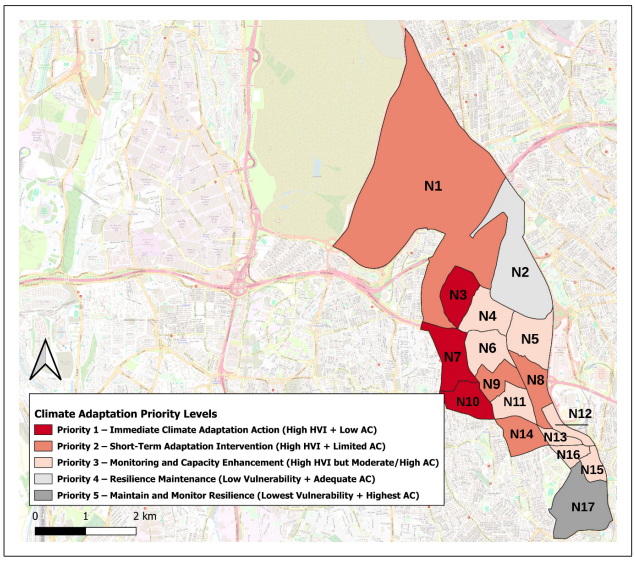

Figure 7. Neighborhood adaptation priority categories derived from the Heat Vulnerability Index–Adaptive Capacity (HVI–AC) Priority Matrix (Design by Authors).

Crucially, spatial interventions should be integrated with socio-economic support mechanisms to protect the most vulnerable residents. Localized Heat Action Plans should prioritize low-income households, older adults, children, and people with chronic health conditions. As demonstrated in several global cities, such frameworks combine early warning systems, accessible cooling centers, resource distribution, and targeted health outreach to reduce heat risks (Uejio et al., 2024; Randazza et al., 2023). Cooling centers, when equitably located and supported by outreach, remain a proven, low-cost measure to lessen heat burden (Bedi et al., 2022; Berisha et al., 2017). Aligning spatial heat-risk mapping with public health and social services can shift municipalities from reactive response to proactive prevention, embedding equity and resilience into local adaptation systems.

At the governance level, Esenler's experience highlights the need to mainstream heat adaptation within Istanbul's broader urban resilience and disaster risk management frameworks. Despite growing policy awareness of climate impacts, extreme heat remains marginally addressed in Türkiye's national and municipal disaster plans, with limited actionable guidance. Integrating heat-risk considerations into urban planning regulations, design standards, and municipal budgeting processes is therefore critical to close this institutional gap, as also emphasized in recent policy analyses highlighting the absence of coordinated frameworks for managing urban heat in Türkiye (Tokaç, 2025). District-level vulnerability maps, such as the HVI produced by this study, can serve as actionable decision-support tools by identifying priority areas for intervention and optimizing the allocation of resources for heat adaptation. City officials could use these maps to target zones for new parks, enhanced infrastructure, or focused social support. For Esenler Municipality, this may include incorporating heat-vulnerability criteria into neighborhood-scale investment decisions, prioritizing adaptation funding for high-risk areas, and coordinating heat-related interventions across planning, environmental management, public health, and social-support departments. Such an approach would help translate vulnerability assessment results into operational planning and resource-allocation decisions. The spatial distribution of heat vulnerability and adaptive capacity observed in Esenler highlights the importance of incorporating equity considerations into future adaptation planning. Similar concerns have been raised by Wang et al. (2025), who demonstrated that urban greening initiatives often disproportionately benefit wealthier districts, worsening supply–demand mismatches and reinforcing socio-ecological inequalities. Their findings underscore the need for policies that explicitly integrate equity considerations into green infrastructure planning to ensure that adaptation investments are directed toward the neighborhoods with the greatest need.

Equity must guide adaptation; the IPCC emphasizes that climate-resilient development requires prioritizing risk reduction, equity, and justice via inclusive governance (IPCC, 2022). In Istanbul, neighborhoods such as Esenler illustrate how socio-economically disadvantaged communities may experience disproportionately higher exposure to heat-related risks, raising important concerns regarding equity in climate adaptation planning. Establishing dedicated adaptation funds or incentives for vulnerable districts and involving residents in participatory planning can ensure that interventions are both adequately financed and tailored to community needs. Such inclusive governance mechanisms would help ensure that local perspectives inform project design and implementation, improving both the fairness and effectiveness of heat adaptation initiatives.

Finally, the Esenler case offers transferable lessons for other rapidly urbanizing cities facing similar challenges. The spatial and socio-environmental characteristics observed in Esenler, marked by dense construction, limited greenery, and low adaptive capacity, are not unique but mirror conditions commonly found in other rapidly growing urban districts. The approach taken in this study, which integrates spatial data with socio-demographic indicators and uses a comparative weighting analysis, provides a replicable model for identifying heat-vulnerable zones in these urban settings. Embedding such vulnerability assessment frameworks into routine urban management and climate action plans can help cities anticipate and mitigate the growing heat risks under a warming climate. Proactively employing data-driven tools to pinpoint hotspots and guide interventions will become increasingly important as extreme heat events become more frequent and intense.

Limitations and Future Directions

Despite its contributions, this study has several limitations. The first limitation concerns the accuracy, temporal scope, and resolution of the Landsat 8–derived LST data. While the 30 m spatial resolution provides valuable insights into neighborhood-scale heat variations, it may not capture micro-scale temperature heterogeneity in Esenler's densely built environment, such as narrow streets, courtyards, or rooftop surfaces. Additionally, the analysis relied on a single-date LST map (13 August 2024) representing peak summer conditions. Although this snapshot effectively identifies spatial hotspots, it limits the generalizability of findings, as it may not capture seasonal dynamics, interannual variability, nighttime heat retention, or extreme heatwave events. Future research could integrate multi-temporal or seasonal satellite imagery, complemented by ground-based temperature monitoring, to improve the temporal robustness and accuracy of heat exposure assessments. A second limitation relates to the spatial aggregation of data at the neighborhood level. Although this scale supports administrative and planning applications, it can obscure intra-neighborhood variations, especially in compact areas where vulnerability may fluctuate significantly over short distances. Future research could adopt parcel- or block-level analyses to better capture spatial inequities and micro-scale heat risks.

Another important limitation involves missing data on building characteristics and health outcomes. Neighborhood-scale information on housing quality, construction materials, energy use, or heat-related morbidity was unavailable. Because neighborhood-level health outcome data are not publicly accessible, this study could not validate the HVI results against observed heat-related illness or mortality patterns. The absence of such data may lead to an underestimation of vulnerability in low-income or poorly built neighborhoods. Incorporating these variables in future assessments would enable a more comprehensive and empirically grounded representation of both structural and physiological vulnerability. Lastly, this study primarily emphasizes structural and environmental indicators, without directly addressing behavioral adaptations or community-level coping strategies that shape lived heat experiences. Integrating qualitative methods, such as interviews or focus groups, would help connect statistical vulnerability with human perception and adaptation behaviors.

In summary, while this research demonstrates the utility of combining Equal and Entropy Weighting in a multi-dimensional HVI framework, its findings should be interpreted in light of data and scale constraints. This study contributes a localized and data-driven assessment that fills a critical gap in Istanbul's urban climate literature, where comprehensive, neighborhood-scale analyses of heat vulnerability have been lacking, particularly for socio-economically disadvantaged districts such as Esenler. Addressing current limitations through finer-resolution, interdisciplinary, and participatory approaches will further strengthen the precision, inclusivity, and policy relevance of future urban heat resilience planning in Esenler, Istanbul, and comparable high-density urban districts.

CONCLUSION

This study developed a comprehensive, neighborhood-scale HVI for Esenler District, Istanbul, integrating environmental exposure, socio-demographic sensitivity, and adaptive capacity within the IPCC vulnerability framework. By combining Equal and Entropy Weighting Methods, it provided both a transparent baseline and a data-driven robustness assessment of indicator weighting, enhancing the robustness and interpretability of vulnerability outcomes. The results reveal pronounced spatial disparities, with vulnerability concentrated in densely built, low-income neighborhoods characterized by limited greenery and reduced adaptive capacity. Beyond its empirical findings, this research contributes methodologically by localizing and comparing alternative weighting approaches within Istanbul's context, addressing a gap in the city's heat-vulnerability literature, which has largely lacked neighborhood-level analyses and comparative weighting assessments. The strong agreement between Equal Weighting and Entropy Weighting results demonstrates that the proposed framework produces robust and consistent vulnerability patterns while remaining transparent and replicable. The Entropy Weighting Method further proved suitable for heterogeneous, small-sample urban datasets, offering a practical complementary approach for similar data-constrained urban environments. The findings underscore the need for targeted climate adaptation strategies, prioritizing green infrastructure expansion, equitable distribution of cooling resources, and socio-economic capacity building in the most heat-vulnerable neighborhoods. The proposed framework is transferable to other districts and cities, as it draws on widely accessible spatial and socio-demographic datasets and adaptable indicator categories consistent with the IPCC structure. Its modular design enables researchers and planners to calibrate indicators, weights, and thresholds according to local data and policy contexts, enhancing replicability across diverse urban settings. Ultimately, this study provides an evidence-based framework for urban heat resilience planning in Istanbul by identifying priority neighborhoods for targeted, equity-oriented adaptation interventions. The HVI–Adaptive Capacity prioritization approach offers decision-makers a practical tool for directing resources toward the communities most vulnerable to heat-related risks, contributing both to Esenler's local adaptation planning and to broader efforts to support equitable climate action in rapidly urbanizing cities.

Appendix: https://jag.journalagent.com/megaron/abs_files/MEGARON-24922/MEGARON-24922_(1)_Appendix-revised.docx

REFERENCES

Adnan, M. S. G., Kabir, I., Hossain, M. A., Chakma, S., Tasneem, S. N., Saha, C. R., ... & Dewan, A. (2024). Heatwave vulnerability of large metropolitans in Bangladesh: An evaluation. *Geomatica, 76*(2), 100020. https://doi.org/10.1016/j.geomat.2024.100020

Alshuwaikhat, H. M., & Aina, Y. A. (2006). GIS-based urban sustainability assessment: The case of Dammam city, Saudi Arabia. *Local Environment*, *11*(02), 141-162. https://doi.org/10.1080/13549830600558432

Bedi, N. S., Adams, Q. H., Hess, J. J., & Wellenius, G. A. (2022). The role of cooling centers in protecting vulnerable individuals from extreme heat. *Epidemiology, 33*(5), 611-615. https://doi.org/10.1097/EDE.0000000000001503

Bektaş, Y., & Sakarya, A. (2023). The relationship between the built environment and climate change: The case of Turkish provinces. *Sustainability*, *15*(2), 1659. https://doi.org/10.3390/su15021659

Berisha, V., Hondula, D., Roach, M., White, J. R., McKinney, B., Bentz, D., ... & Goodin, K. (2017). Assessing adaptation strategies for extreme heat: a public health evaluation of cooling centers in Maricopa County, Arizona. *Weather, climate, and society*, *9*(1), 71-80. https://doi.org/10.1175/WCAS-D-16-0033.1

Bhattacharjee, S., Gerasimova, E., Imbert, C., Tencar, J., & Rotondo, F. (2019, June). *Assessment of different methodologies for mapping urban heat vulnerability for Milan, Italy*. In IOP conference series: Earth and environmental science (Vol. 290, No. 1, p. 012162). IOP Publishing. https://doi.org/10.1088/1755-1315/290/1/012162

Bu, S., Smith, K. L., Masoud, F., & Sheinbaum, A. (2024). Spatial distribution of heat vulnerability in Toronto, Canada. *Urban Climate*, *54*, 101838. https://doi.org/10.1016/j.uclim.2024.101838

Can, G., Şahin, Ü., Sayılı, U., Dubé, M., Kara, B., Acar, H. C., ... & Gosselin, P. (2019). Excess mortality in Istanbul during extreme heat waves between 2013 and 2017. *International journal of environmental research and public health, 16*(22), 4348. https://doi.org/10.3390/ijerph16224348

Cangüzel, A., & Coşkun Hepcan, Ç. (2024). Climate change vulnerability assessment of Karşıyaka, İzmir. *Natural Hazards, 120*(15), 14869–14888. https://doi.org/10.1007/s11069-024-06798-5

Chen, H., Dong, N., Cao, Q., Chen, G., & Zheng, X. (2025a). Spatial-temporal assessment of urban heat vulnerability analysis based on local climate zone in Guangzhou-Foshan metropolis. *Sustainable Cities and Society, 130*, 106618. https://doi.org/10.1016/j.scs.2025.106618

Chen, J., Shi, X., Shi, Y., & Delina, L. L. (2025b). Assessing heat vulnerability risk of Jinan and Guangzhou's older populations based on multisource remote sensing data. *Building and Environment, 271*, 112622. https://doi.org/10.1016/j.buildenv.2025.112622

Cheng, W., Li, D., Liu, Z., & Brown, R. D. (2021). Approaches for identifying heat-vulnerable populations and locations: A systematic review. *Science of The Total Environment, 799*, 149417. https://doi.org/10.1016/j.scitotenv.2021.149417

Climate Data. 2025. Climate summary for Esenler, Turkey. Retrieved September 28, 2025, from https://en.climate-data.org/asia/turkey/istanbul/esenler-53158/

Cresswell, K. (2023). A Florida urban heat risk index: Assessing weighting and aggregation approaches. *Urban Climate*, *51*, 101646. https://doi.org/10.1016/j.uclim.2023.101646

Dogru, A. O., Kahraman, A., Seker, D. Z., & Sivri, N. (2019). GIS based evaluation of social determinants of children's health in Turkey: Case study of Istanbul. *Environmental research*, *179*, 108753. https://doi.org/10.1016/j.envres.2019.108753

Endeksa. (2025). *Neighborhood-level socioeconomic and demographic data: Household income, age distribution, education level, and illiteracy rates*. Retrieved July 17, 2026, from https://www.endeksa.com/en/analysis/turkiye/demography

Fall, S., Coulibaly, K., Quansah, J., & El Afandi, G. (2023). Differential urban heat vulnerability: the tale of three Alabama cities. *Urban Science, 7*(4), 121. https://doi.org/10.3390/urbansci7040121

Guo, F., Zheng, R., Zhao, J., Zhang, H., & Dong, J. (2024). Framework of street grid-based urban heat vulnerability assessment: Integrating entropy weight method and BPNN model. *Urban Climate*, *56*, 102067. https://doi.org/10.1016/j.uclim.2024.102067

Hammer, J., Ruggieri, D. G., Thomas, C., & Caum, J. (2020). Local extreme heat planning: an interactive tool to examine a heat vulnerability index for Philadelphia, Pennsylvania. *Journal of Urban Health, 97*(4), 519-528. https://doi.org/10.1007/s11524-020-00443-9

Ho, H. C., Tong, S., Zhou, Y., Hu, K., Yang, X., & Yang, Y. (2025). Mapping Heat Vulnerability and Heat Risk for Neighborhood Health Risk Management in Urban Environment? Challenges and Opportunities. *Current environmental health reports*, *12*(1), 14. https://doi.org/10.1007/s40572-025-00478-7

Hossain, I., Rana, M. S., Haque, A. M., & Al Masud, A. (2024). Urban household adaptation to extreme heatwaves: health impacts, socio-economic disparities and sustainable strategies in Rajshahi. *Discover Sustainability, 5*(1), 518. https://doi.org/10.1007/s43621-024-00697-2

Inostroza, L., Palme, M., & De La Barrera, F. (2016). A heat vulnerability index: spatial patterns of exposure, sensitivity and adaptive capacity for Santiago

de Chile. *PLOS one, 11*(9), e0162464. https://doi.org/10.1371/journal.pone.0162464

Intergovernmental Panel on Climate Change (IPCC). (2014). *Climate change 2014: Impacts, adaptation, and vulnerability. Contribution of Working Group II to the Fifth Assessment Report of the Intergovernmental Panel on Climate Change*. Cambridge University Press. https://doi.org/10.1017/CBO9781107415379

Intergovernmental Panel on Climate Change (IPCC). (2022). *Climate change 2022: Impacts, adaptation and vulnerability. Working Group II contribution to the Sixth Assessment Report of the Intergovernmental Panel on Climate Change*. Cambridge University Press.https://doi.org/10.1017/9781009325844

Istanbul Metropolitan Municipality. (2024). *Istanbul Green Area Management System (YAYSİS) – Interactive green-space map*. Retrieved Juy 17, 2026, from https://yaysis.ibb.gov.tr/portal/apps/MapSeries/index.html?appid=e73e1b46060b45d0bf654c787673d3b5

Jiang, S. (2023). Compound heat vulnerability in the record-breaking hot summer of 2022 over the Yangtze River Delta Region. *International Journal of Environmental Research and Public Health, 20*(8), 5539. https://doi.org/10.3390/ijerph20085539

Kamal, N. I. A., Ash'aari, Z. H., Abdullah, A. M., Kusin, F. M., Mohamat Yusuff, F., Sharaai, A. H., ... & Mohd Ariffin, N. A. (2022). Extreme heat vulnerability assessment in tropical region: A case study in Malaysia. *Climate and Development, 14*(5), 472–486. https://doi.org/10.1080/17565529.2021.1937030

Khorrami, B., & Gündüz, O. (2019). Uzaktan Algılama ve CBS'nin Yüzey Sıcaklığı ve Kentsel Isı Adası Tespit ve Analizinde Uygulanması. *Meteorolojik Uzaktan Algılama Sempozyumu (UZALMET 2019)* Antalya, Türkiye.

Kim, Y., Li, D., Xu, Y., Zhang, Y., Li, X., Muhlenforth, L., ... & Brown, R. (2023). Heat vulnerability and street-level outdoor thermal comfort in the city of Houston: Application of google street view image derived SVFs. *Urban Climate, 51*, 101617. https://doi.org/10.1016/j.uclim.2023.101617

Kimmich, C., Weyerstraß, K., Czypionka, T., Fauster, N. F., Kinner, M., Laa, E., ... & Poledna, S. (2025). Economic impact of labor productivity losses induced by heat stress: an agent-based macroeconomic approach. *Climatic Change, 178*(3), 36. https://doi.org/10.1007/s10584-025-03879-7

Kitchley, J. L. (2024). A framework to assess the contextual composite heat vulnerability index for a heritage city in India-A case study of Madurai. *Sustainable Cities and Society*, *101*, 105119. https://doi.org/10.1016/j.scs.2023.105119

Kuru, A., & Okay, B. B. (2025). Investigating the relationship between urban growth pattern and urban heat islands: the case of Istanbul, Turkey. *Environmental Earth Sciences*, *84*(1), 1–15. https://doi.org/10.1007/s12665-024-12064-5

Lai, W., Qiu, Y., Tang, Q., Xi, C., & Zhang, P. (2023). The effects of temperature on labor productivity. *Annual Review of Resource Economics, 15*(1), 213–232. https://doi.org/10.1146/annurev-resource-101222-125630

Leal Filho, W., Icaza, L. E., Neht, A., Klavins, M., & Morgan, E. A. (2018). Coping with the impacts of urban heat islands. A literature based study on understanding urban heat vulnerability and the need for resilience in cities in a global climate change context. *Journal of Cleaner Production*, *171*, 1140–1149. https://doi.org/10.1016/j.jclepro.2017.10.086

Li, F., Yigitcanlar, T., Nepal, M., Nguyen, K., Dur, F., & Li, W. (2024). Assessing heat vulnerability and multi-dimensional inequity: Lessons from indexing the performance of Australian capital cities. *Sustainable Cities and Society, 115*, 105875. https://doi.org/10.1016/j.scs.2024.105875

Li, F., Yigitcanlar, T., Nepal, M., Nguyen, K., Dur, F., & Li, W. (2025). Mapping heat vulnerability in Australian capital cities: A machine learning and multi-source data analysis. *Sustainable Cities and Society, 119*, 106079. https://doi.org/10.1016/j.scs.2024.106079

Li, F., Yigitcanlar, T., Nepal, M., Thanh, K. N., & Dur, F. (2022). Understanding urban heat vulnerability assessment methods: A PRISMA review. *Energies*, *15*(19), 6998. **https://doi.org/10.3390/en15196998**

Lopes, H. S., Silva, P. F., Pinto, B. G., Cuevas, P. D., Ribeiro, V., & Remoaldo, P. (2025). Urban heat stress in the context of socioeconomic and environmental challenges: Heat risk analysis and online surveys in northwestern Portugal. *International Journal of Disaster Risk Reduction, 120*(10538), 105384. https://doi.org/10.1016/j.ijdrr.2025.105384

Ma, D., Wang, Y., Zhou, D., & Zhu, Z. (2023). Cooling effect of the pocket park in the built-up block of a city: a case study in Xi'an, China. *Environmental Science and Pollution Research*, *30*(9), 23135–23154. https://doi.org/10.1007/s11356-022-23809-9

Macharia, C. W., & Kiage, L. (2025). Examining the nexus of social vulnerability, land cover dynamics, and heat exposure in Reno, Nevada, USA. *Remote Sensing Applications: Society and Environment, 37*, 101400. https://doi.org/10.1016/j.rsase.2024.101400

Mallen, E., Stone, B., & Lanza, K. (2019). A methodological assessment of extreme heat mortality modeling and heat vulnerability mapping in Dallas, Texas. *Urban Climate*, *30*, 100528. https://doi.org/10.1016/j.uclim.2019.100528

Méndez-Lázaro, P., Muller-Karger, F. E., Otis, D., McCarthy, M. J., & Rodríguez, E. (2018). A heat vulnerability index to improve urban public health management

in San Juan, Puerto Rico. *International journal of biometeorology, 62*, 709-722. https://doi.org/10.1007/s00484-017-1319-z

Ministry of Labour and Social Security. (2024, December 24). *The net minimum wage for 2025 has been determined as 22,104 TL*. Republic of Türkiye Ministry of Labour and Social Security.

Mundfrom, D. J., Shaw, D. G., & Ke, T. L. (2005). Minimum sample size recommendations for conducting factor analyses. *International journal of testing*, *5*(2), 159-168. https://doi.org/10.1207/s15327574ijt0502_4

Munoz-Pizza, D. M., Sanchez-Rodriguez, R. A., & Gonzalez-Manzano, E. (2023). Linking climate change to urban planning through vulnerability assessment: The case of two cities at the Mexico-US border. *Urban Climate, 51*, 101674. https://doi.org/10.1016/j.uclim.2023.101674

National Smart City Open Data Platform. (2024). *Health-service locations in Istanbul* [Spatial dataset]. https://ulusalveri.sehirveyonetim.org.tr

Oh, K. Y., Lee, M. J., & Jeon, S. W. (2017). Development of the Korean climate change vulnerability assessment tool (VESTAP)—Centered on health vulnerability to heat waves. *Sustainability, 9*(7), 1103. https://doi.org/10.3390/su9071103

Okumuş, D. E. (2025). Decoding nonlinear dynamics in urban heat vulnerability: A multi-model framework for socio-spatial responses to extreme heat. *Sustainable Cities and Society, 135*, 106995. https://doi.org/10.1016/j.scs.2025.106995

Okumuş, D. E., & Terzi, F. (2021). Evaluating the role of urban fabric on surface urban heat island: The case of Istanbul. *Sustainable Cities and Society*, *73*, 103128. https://doi.org/10.1016/j.scs.2021.103128

Parker, C., Mahlasi, C., Govindasamy, T., Radebe, L., Brink, N. B., Jack, C., ... & Makhanya, S. (2025). Quantifying intra-urban socio-economic and environmental vulnerability to extreme heat events in Johannesburg, South Africa. *International Journal of Biometeorology, 69*, 2501–2517. https://doi.org/10.1007/s00484-025-02971-y

Patel, S., Indraganti, M., & Jawarneh, R. N. (2024). Land surface temperature responses to land use dynamics in urban areas of Doha, Qatar. *Sustainable Cities and Society*, *104*, 105273. https://doi.org/10.1016/j.scs.2024.105273

Raja, D. R., Hredoy, M. S. N., Islam, M. K., Islam, K. A., & Adnan, M. S. G. (2021). Spatial distribution of heatwave vulnerability in a coastal city of Bangladesh. *Environmental Challenges, 4*, 100122. https://doi.org/10.1016/j.envc.2021.100122

Ramsey, V., Scannell, C., Dunbar, T., Sanderson, M., & Lowe, J. A. (2024). Co-producing an urban heat climate service for UK cities: A case study of Belfast, Northern Ireland. *Climate Services, 34*, 100464. https://doi.org/10.1016/j.cliser.2024.100464

Randazza, J. M., Hess, J. J., Bostrom, A., Hartwell, C., Adams, Q. H., Nori-Sarma, A., ... & Errett, N. A. (2023). Planning to reduce the health impacts of extreme heat: A content analysis of heat action plans in local United States jurisdictions. *American journal of public health*, *113*(5), 559-567. https://doi.org/10.2105/AJPH.2022.307217)

Ren, Z., Zhao, H., Fu, Y., Xiao, L., & Dong, Y. (2022). Effects of urban street trees on human thermal comfort and physiological indices: a case study in Changchun city, China. *Journal of Forestry Research*, *33*(3), 911-922. https://doi.org/10.1007/s11676-021-01361-5

Salleh, S. A., Isa, N. A., Siman, N. A., Zakaria, N. H., Pintor, L. L., Yaman, R., & Dom, N. C. (2023). The Development of the Vulnerability Index (VI) using Principal Component Analysis (PCA). *International Journal of Sustainable Construction Engineering and Technology, 14*(5), 16-36. https://doi.org/10.30880/ijscet.2023.14.05.002

Sarı, E. N., Nouri, A. S., Ekşi, M., & Matzarakis, A. (2025). Quantifying thermo-physiological stress exposure during extreme events: Developing a morphological case study in Istanbul. *Building and Environment, 267*, 112304. https://doi.org/10.1016/j.buildenv.2024.112304

Sari, E., Öztürk, S. P., & As, İ. (2022). The Resilient City of The Future: Esenler Nar Innovation District. *Çevre Şehir ve İklim Dergisi, 1*(2), 119-146.

Shartova, N., Mironova, E., Varentsov, M., Grischenko, M., & Konstantinov, P. (2024). Exploring intra-urban thermal stress vulnerability within 15-minute city concept: Example of heat waves 2021 in Moscow. *Sustainable Cities and Society*, *114*, 105729. https://doi.org/10.1016/j.scs.2024.105729

Shen, P., Ji, Y., Li, Y., Wang, M., Cui, X., & Tong, H. (2025). Combined impact of climate change and heat island on building energy use in three megacities in China. *Energy and Buildings*, *331*, 115386. https://doi.org/10.1016/j.enbuild.2025.115386

Sianturi, R. S., Aknuranda, I., & Perdanakusuma, A. R. (2023, October*). Estimating Heat Vulnerability Index (HVI) in Indonesia*. In Proceedings of the 8th International Conference on Sustainable Information Engineering and Technology (pp. 431-438). https://doi.org/10.1145/3626641.3626676

Singh, A. M. (2023). Mapping of heat vulnerability in Indian Urban Centres under threat of global warming. *Journal of Applied and Natural Science, 15*(4), 1514. https://doi.org/10.31018/jans.v15i4.5039

Sun, Y., Li, Y., Ma, R., Gao, C., & Wu, Y. (2022). Mapping urban socio-economic vulnerability related to heat risk: A grid-based assessment framework by combing

the geospatial big data. *Urban Climate*, 43, 101169. https://doi.org/10.1016/j.uclim.2022.101169

Şeker, M., Baypınar, M. B., Çelikbıçak, G., & Özbay, B. K. (2022). Quality of life index: *Istanbul 2020. İstanbul İktisat Dergisi, 72*(2), 543-568. https://doi.org/10.26650/ISTJECON2022-1115346

Tabachnick, B. G., & Fidell, L. S. (2013). Using multivariate statistics (ed., Vol. 6). *MA: Pearson*.

Tokaç, F. Z. (2025, July). Managing an Invisible Disaster: Developing a Comprehensive Heat Action Plan for Istanbul. In *Proceedings of the international conference of contemporary affairs in architecture and urbanism-ICCAUA* (Vol. 8, No. 1, pp. 587-593). https://doi.org/10.38027/ICCAUA2025EN0305

Tran, D. N., Doan, V. Q., Nguyen, V. T., Khan, A., Thai, P. K., Cunrui, H., ... & Phung, D. (2020). Spatial patterns of health vulnerability to heatwaves in Vietnam. *International journal of biometeorology, 64*(5), 863-872. https://doi.org/10.1007/s00484-020-01876-2

Turkish Statistical Institute (TÜİK). (2023). *Address-based population registration system (ADNKS) results by neighborhood*. Retrieved July 17, 2026, from https://veriportali.tuik.gov.tr/en/press/49684

Uejio, C. K., Gilbert, J., Ahn, Y., Martella, L., Hu, L., & Marturano, J. (2024). Rapidly developing a community-and evidence-based heat action plan. *Bulletin of the American Meteorological Society*, *105*(5), E848-E863. https://doi.org/10.1175/BAMS-D-23-0055.1

Vésier, C., & Urban, A. (2023). Gender inequalities in heat-related mortality in the Czech Republic. *International journal of biometeorology*, *67*(8), 1373-1385. https://doi.org/10.1007/s00484-023-02507-2

Wang, J., Li, Y., Liu, W., & Gou, A. (2024). Spatial and temporal evolution characteristics and factors of heat vulnerability in the Pearl River Delta urban agglomeration from 2001 to 2022. *Heliyon, 10*(13), e34116

Wang, J., Zhou, W., McPhearson, T., Cook, E. M., Herreros-Cantis, P., & Liu, J. (2025). Socio-ecological impacts of the investment of urban nature in heat mitigation for two megacities. *Earth's Future, 13*(6), e2025EF005976. https://doi.org/10.1029/2025EF005976

WeatherSpark. (2025). *Average weather in Esenler, Turkey*. Retrieved September 28, 2025, from https://weatherspark.com/y/95436/Average-Weather-in-Esenler-Turkey-Year-Round

Weber, S., Sadoff, N., Zell, E., & de Sherbinin, A. (2015). Policy-relevant indicators for mapping the vulnerability of urban populations to extreme heat events: A case study of Philadelphia. *Applied Geography, 63*, 231–243. https://doi.org/10.1016/j.apgeog.2015.07.006

World Health Organization. (2010). *Monitoring the Building Blocks of Health Systems: A Handbook of Indicators and Their Measurement Strategies*. Retrieved July 17, 2026, from https://cdn.who.int/media/docs/default-source/service-availability-and-readinessassessment%28sara%29/related-links-%28sara%29/who_mbhss_2010_section1_web.pdf

World Health Organization. Regional Office for Europe. (2016). *Urban green spaces and health: A review of evidence.* Retrieved July 17, 2026, from https://iris.who.int/handle/10665/345751

Yang, Y., & Zhao, N. (2023). Vulnerability assessment of urban agglomerations to the risk of heat waves in China since the 21st century. *Environmental Pollution*, *336*, 122443. https://doi.org/10.1016/j.envpol.2023.122443

Yazar, M., Daloglu, C. I., Can Iban, M.,& Bilgilioglu S.S. (2023). The green divide and heat exposure: Urban transformation projects in Istanbul. *Frontiers in Environmental Science, 11*, 1265332. https://doi.org/10.3389/fenvs.2023.1265332

Yılmaz, M., Çulpan, H. C., Can, G., Toros, H., & Tayanç, M. (2024). Environment, development, and health: the vulnerability of sub-populations in İstanbul to heat extremes. *Environment, Development and Sustainability*, *2024*, 1–23. https://doi.org/10.1007/s10668-024-05828-3

Zaeemdar, S., & Baycan, T. (2017). Analysis of the relationship between Urban Heat Island and land cover in Istanbul through Landsat 8 OLI. *Journal of Earth Science & Climatic Change, 8*(11), 1000423.https://doi.org/10.4172/2157-7617.1000423

Zeng, P., Sun, F., Shi, D., Liu, Y., Zhang, R., Tian, T., & Che, Y. (2022). Integrating anthropogenic heat emissions and cooling accessibility to explore environmental justice in heat-related health risks in Shanghai, China. *Landscape and Urban Planning, 226*, 104490. https://doi.org/10.1016/j.landurbplan.2022.104490

Zhang, M., Wang, H., Jin, W., & Dijk, M. P. V. (2019). Assessing heat wave vulnerability in Beijing and its districts, using a three dimensional model. *International Journal of Global Warming, 17*(3), 297-314. https://doi.org/10.1504/IJGW.2019.098524

Zhang, R., Yang, J., Ma, X., Xiao, X., & Xia, J. C. (2023). Optimal allocation of local climate zones based on heat vulnerability perspective. *Sustainable Cities and Society*, *99*, 104981. https://doi.org/10.1016/j.scs.2023.104981

Zhang, W., McManus, P., & Duncan, E. (2018). A raster-based subdividing indicator to map urban heat vulnerability: A case study in sydney, australia. *International journal of environmental research and public health, 15*(11), 2516. https://doi.org/10.3390/ijerph15112516

Zhou, S. Q., Yu, Z. W., Ma, W. Y., Yao, X. H., Xiong, J. Q., Ma, W. J., ... & Zhao, B. (2025a). Vertical canopy

structure dominates cooling and thermal comfort of urban pocket parks during hot summer days. *Landscape and Urban Planning*, *254*, 105242. https://doi.org/10.1016/j.landurbplan.2024.105242

Zhou, Y., Larochelle, L., Khan, F. A., & Pilote, L. (2025b). Sex differences in the impact of extreme heat on cardiovascular disease outcomes: a systematic review and meta-analysis. *Environmental Health, 24*(1), 20. https://doi.org/10.1186/s12940-025-01175-6

Zuhra, S. S., Tabinda, A. B., & Yasar, A. (2019). Appraisal of the heat vulnerability index in Punjab: a case study of spatial pattern for exposure, sensitivity, and adaptive capacity in megacity Lahore, Pakistan. *International journal of biometeorology*, *63*, 1669-1682. https://doi.org/10.1007/s00484-019-01784-0